Simple Methods for Estimating Required SNR in Dual-Polarized MIMO Systems Under Limited XPD

Sungjun Ahn, *Member, IEEE*, and Sung-Ik Park, *Fellow, IEEE*

***Abstract*—This paper presents simple semi-analytical methods for estimating the required carrier-to-noise ratio (CNR) in multi-input multi-output (MIMO) broadcasting systems. The estimates are derived according to cross-polarization discrimination (XPD) level of the transmission channel, thereby evaluating the impact of cross-polarization interference. The proposed models convert known single-input single-output (SISO) system performance, e.g., CNR threshold measurements in ATSC A/327 [Annex A, 1], into the CNR required in MIMO transmission. Two classes of estimation are developed: one assuming perfect channel knowledge (Class P), and the other accounting for channel estimation errors and pilot boosting (Class E). In addition to the conventional single-layer configuration, estimations under layered division multiplexing (LDM) configurations are also addressed, where every layer is assumed to use MIMO. Closed-form expressions are provided for both layered and non-layered MIMO scenarios. The models offer a lightweight alternative to full-system simulations, enabling early-stage design evaluation and practical system planning in cross-polarized environments.**

***Index Terms*—Cross-polarized MIMO, cross-polarization discrimination (XPD), threshold of visibility (ToV).**

I. Introduction

A. Background and Motivation

TERRESTRIAL broadcasting has entered a new era, one defined by the real-world deployment of multiple-input multiple-output (MIMO) technology [3], [4], [5], [6], [7]. MIMO has been a cornerstone of wireless communications, offering dramatic gains in throughput and spectral efficiency in unicast environments [8]. Yet despite its theoretical promise, MIMO has long remained unrealized in commercial broadcast systems, constrained by the unique challenges of wide-area, one-to-many delivery [9], [10]. While such technical challenges are increasingly seen as manageable, MIMO adoption in digital television (DTV) has been held back more by legacy compatibility and cost constraints than by fundamental limitations [11], [12], [13].

That landscape is now changing. Brazil's *TV 3.0* project [14], [15], a national initiative to redefine the country's broadcasting standard,[1] has placed MIMO support at the core of its physical-layer requirements [16]. This mandate was established from the ground up, and in line with it, the combined use of layered division multiplexing (LDM) and MIMO has also been formally required. Both of those requirements aim to amplify spectral efficiency against Brazil's congested spectrum environment [17], [18], [19].

In response, Advanced Television Systems Committee (ATSC) has revised ATSC 3.0 physical-layer specifications to make MIMO functionality practical and to extend it through the integration of additional features [3], [20], [21]—including *layered MIMO* techniques, i.e., operational designs that combine LDM and MIMO[2] [7], [22]. Real-world implementations and field trials have since validated the system's feasibility [23], [24], [25], ultimately leading to the selection of ATSC 3.0 as the winning proposal for TV 3.0 [14], [26], [27]. With deployment already in motion, MIMO broadcasting is no longer hypothetical—it is happening.

This evolution brings new performance questions to the forefront. As the first national-scale deployment of MIMO broadcasting, the rollout of TV 3.0 faces a lack of prior data to inform network planning and design. Conventional single-input single-output (SISO) systems benefit from a wealth of legacy data that guides coverage prediction [28], [29], [30], [31], [32], [33], [34]. The so-called *threshold of visibility (ToV)*, i.e., the minimum carrier-to-noise ratio (CNR)[3] required for successful reception, has been thoroughly characterized over decades of development. For example, ATSC A/327 [1] Annex A provides a comprehensive collection of computer simulations, laboratory tests, and field measurements detailing ToV levels for every modulation and coding (ModCod) combination defined in ATSC 3.0. Broadcasters have also accumulated empirical knowledge through years of managing SISO-based networks.

In contrast, the MIMO sector is still short of comparable reference data, and this shortage impedes prompt network rollout. MIMO ToV values deviate from their SISO counterparts

Received 2 November 2025; revised 9 March 2026; accepted 13 March 2026. Date of publication 21 April 2026; date of current version 9 June 2026. This work was supported by the Institute of Information and Communications Technology Planning and Evaluation (IITP) funded by Korean Government Ministry of Science and ICT (MSIT) through the Development of Receiver Chip for ATSC 3.0 Mobile Broadcast under Grant RS-2023-00224660. *(Corresponding author: Sungjun Ahn.)*

The authors are with the Media Research Division, Electronics and Telecommunications Research Institute (ETRI), Yuseong-gu, Daejeon 34129, South Korea (e-mail: sjahn@etri.re.kr; psi76@etri.re.kr).

Digital Object Identifier 10.1109/TBC.2026.3680043

[1]The new standard is referred to as *TV 3.0* or *DTV+*, and the project is led by SBTVD Forum. As of this writing, TV 3.0 has adopted ATSC 3.0 for its physical layer and is poised for deployment.

[2]A/322 already included basic definitions of MIMO operations prior to this amendment [21], but lacked several essential details and did not support integration with LDM, transmitter identification [35], [36], or channel bonding.

[3]To avoid confusion, this paper uses a term *CNR* instead of signal-to-noise ratio (SNR). CNR is defined here as the total received signal power per polarization branch (including the cross-polarized component) over the noise floor, i.e., a pre-equalization SNR measured prior to MIMO equalization.

because spatial multiplexing introduces an additional degree of freedom and, consequently, additional loss factors. A primary issue is cross-polarization interference (XPI). Current broadcast MIMO architectures exploit dual, orthogonal polarizations to convey two spatial streams [4]; however, the achievable gain is governed by the channel's cross-polarization discrimination (XPD) [37].

Real-world XPDs are generally limited: Reflections in non-line-of-sight (NLoS) propagation paths convert polarization, and residual isolation in real antennas leaves non-negligible leakage between the polarization paths [38], [39]. These impairments raise the required CNR in MIMO systems even when all other parameters, e.g., ModCod, remain unchanged. MIMO equalization yet isolates the *polarization signals* but high XPD drags it from perfection, and even degrades the underlying channel estimation accuracy.

An exhaustive measurement campaign—similar to the SISO effort in A/327 Annex A—might solve this problem, but the MIMO test matrix grows combinatorially with XPD setting alongside other existing profiles. Field and lab studies [23], [24], [25], [40], [41], [42], [43] that conducted performance evaluations found this issue to be a serious challenge. For example, conventions for SISO have addressed a handful of representative channel models, e.g., Additive white Gaussian noise (AWGN), RL20, RC20, TU-6 models [1], [30], but now MIMO needs to add XPD dimension to each model. Adding the increased complexity inherent in MIMO simulations and measurements themselves, the burdens render such brute-force approaches prohibitive for time-critical TV 3.0 deployment.

Against this backdrop, a lightweight alternative is needed; one that avoids rebuilding an exhaustive measurement dataset. This paper therefore introduces a tractable, formula-driven framework for predicting MIMO ToV—an aspect largely absent from prior MIMO-theoretic studies. The proposed is a closed-form procedure that extrapolates MIMO ToVs from the extensive SISO data already in hand, achieving simplicity without sacrificing reliability. We bridge well-characterized SISO measurements to realistic MIMO performance projections under XPD conditions. Notably, this approach applies to virtually any physical-layer configuration, including ModCod settings, and is even agnostic to standard specifications. Furthermore, this paper provides ToV estimators also for layered MIMO[4] transmissions, a feature widely recognized as pivotal for the upcoming era.

This work has been developed in response to practical requests received from ATSC and Brazilian TV 3.0 stakeholders, and has been incorporated into ATSC A/327 [1]. By means of the proposed methods, designers gain a compact toolkit for full-scale radio map simulation of MIMO transmissions. XPD-aware ToV estimates can be plugged directly into coverage engines to project cell contours on real terrain for any mix of system setups.[5] The same figures will further feed various design tasks including link budgets, interference studies, and channel allocation plans. Receiver development will also benefit, aided by a clear guide for algorithm validation and implementation-loss evaluation. Amplifying this versatility, the proposed approach can readily and generally be transferred to other wireless systems as well.

B. Main Contributions

This paper proposes compact, closed-form methods for estimating the ToV required for MIMO broadcast reception, namely the CNR threshold for quasi-error-free (QEF) performance. Methodologically, SISO ToVs are converted into their MIMO counterparts; equivalently, we illustrate the impact of XPI as a ToV penalty.[6] The main contributions are as follows:

- Tractable, closed-form prediction models are proposed to derive the required CNRs in cross-polarized MIMO systems.
  - An efficient approach is proposed: Mapping known SISO ToVs (such as those measured in [1]) into equivalent MIMO performance estimates.
- ToV estimates are derived as a function of channel XPD and span standard AWGN, Rayleigh, and Rician channel models that capture practical propagation conditions.
- Two classes of estimation procedures are developed according to the available channel knowledge:
  - Class P: Assumes perfect channel state information at the receiver (CSIR).
  - Class E: Incorporates channel estimation error via a theoretical minimum mean-square error (MMSE) estimator and accounts for pilot-boosting effects.
- ToV estimators for LDM+MIMO configurations are developed, yielding the threshold CNR for each layer.

C. Notation and Outline

A brief remark on notation is in order. The following conventions are used throughout the remainder of this paper.

τ_{M}	Required CNR estimate in a MIMO system (linear-scale), i.e., the estimated MIMO ToV.
τ_{S}	Reference CNR requirement measured in SISO systems (linear-scale), i.e., the reference SISO ToV.
μ	Channel model parameter s.t. $\mu \in \{\mathtt{AWGN}, \mathtt{RL}, \mathtt{RC}\}$.
Θ_{XPD}	Channel XPD parameter defined as subject to the channel model.
χ_L^{dB}	dB-scale channel XPD evaluated in the LoS part of MIMO channel.
χ_N^{dB}	dB-scale channel XPD evaluated in the NLoS part of MIMO channel.
δ	Enhanced layer injection level (linear-scale).
F_{PB}	Pilot boosting applied to the scattered pilots (dB-scale).
$\mathbb{E}_X[\,\cdot\,]$	Statistical expectation over the ensemble of X.
$\det(\mathbf{A})$	Determinant of a matrix $\mathbf{A}$.
$\mathbf{I}$	Identity matrix.
$\log(\cdot)$	Natural logarithm.
$\lVert\cdot\rVert_{\mathrm{F}}$	Frobenius norm.
$\mathcal{CN}(m, \sigma^2)$	Complex Gaussian distribution with mean m and variance σ^2.

[4]Specifically, this paper covers *layered MIMO Type A* in A/322 [20].

[5]The proposed methods have been integrated into the commercial network coverage planning software PROGIRA® Plan.

[6]Note that the throughput nearly doubles while MIMO calls for this ToV markup. Other modulation and encoding schemes are assumed as unchanged.

Vectors are denoted by lower-case bold letters, while matrices are denoted by upper-case bold letters. Other notations follow standard usage unless otherwise specified.

The rest of this article is organized as follows. Section II introduces the system models that underpin the proposed ToV estimators. Sections III and IV directly present the results on how to estimate the threshold CNRs, while addressing the perfect CSIR case and MMSE-estimated CSIR case, respectively. Sections V and VI detail the derivations behind these results, and Section VII explains the relationship between XPD concepts. Numerical results are presented in Section VIII, and Section IX concludes the paper with final remarks.

II. System Model and Organization

This section describes the system model considered. Section II-A presents an overview; Section II-B details the channel models thereof; Section II-C outlines the organization and class structure of the proposed estimation procedures.

A. System Description

The tackled is a 2×2 wireless MIMO system that employs cross-polarized transmission. Spatial multiplexing is realized over two orthogonal polarizations: for example, vertical and horizontal in the linear/planar case, or left- and right-hand senses in the circular case. Here, the term *polarization* refers to the orientation of a radio wave's electric field vector relative to the horizon as viewed from the antenna. For clarity, the two orthogonal polarizations will be designated as polarization #1 (*pol* #1) and polarization #2 (*pol* #2) throughout this paper, consistent with the notation in [20].

That is, each encoded message block, namely a codeword, is split across *pol* #1 and *pol* #2 transmissions. Precisely, the bit-interleaved coded modulation (BICM) chain operates as follows: A codeword is first generated, then demultiplexed into two bit streams dedicated to *pol* #1 and *pol* #2, respectively; each stream is subsequently mapped to its own sequence of constellation symbols.

The baseline scheme is a single-layer transmission without LDM, referred to hereafter as non-layered (or single-layer) MIMO. When this single-layer MIMO is used, the received baseband signal can be expressed as

$$\begin{aligned}\mathbf{y} &= \mathbf{H}\mathbf{x} + \mathbf{n} \\ &= \begin{bmatrix} h_{00} & h_{10} \\ h_{01} & h_{11} \end{bmatrix} \mathbf{x} + \mathbf{n}, \end{aligned} \tag{1}$$

where $\mathbf{x} = [x_0, x_1]^T \in \mathbb{C}^{2\times 1}$ denotes the power-scaled transmit symbol[7] vector consisting of the *pol* #1 component x_0 and the *pol* #2 component x_1; $\mathbf{H} \in \mathbb{C}^{2\times 2}$ denotes the MIMO channel matrix for small-scale fading with $\mathbb{E}_{\mathbf{H}}[|h_{00}|^2] + \mathbb{E}_{\mathbf{H}}[|h_{10}|^2] = \mathbb{E}_{\mathbf{H}}[|h_{01}|^2] + \mathbb{E}_{\mathbf{H}}[|h_{11}|^2] = 1$; and $\mathbf{n} = [n_0, n_1]^T \in \mathbb{C}^{2\times 1}$ denotes the additive white Gaussian noise (AWGN) vector consisting of the *pol* #1 component n_0 and the *pol* #2 component n_1. Note that $\mathbf{x} \sim \mathcal{CN}(\mathbf{0}, P_R\mathbf{I})$ includes large-scale fading (e.g., path-loss and shadowing), which means that $P_R \geq 0$ represents the received signal power on each polarization.[8] On the other hand, $\mathbf{n}$ conforms to $\mathcal{CN}(\mathbf{0}, \sigma_n^2\mathbf{I})$, where $\sigma_n^2 > 0$ indicates the system noise level. The statistical characteristics of $\mathbf{H}$ will later be detailed in Section II-B.

The results in this paper are theoretical estimates relying on optimal MIMO equalization assumption at the receiver. Maximum likelihood (ML) MIMO equalization is assumed for the calculation model, so minor implementation losses can potentially be added when other MIMO equalization schemes are used, such as MMSE methods.

§ *Remark: Issues in measuring MIMO signal strength*

In contrast to the SISO case, MIMO systems raise a measurement question about the threshold signal power required for successful decoding. The problem stems from the presence of multiple antenna branches. In SISO systems, the SNR maps directly to the received field strength, which field engineers can measure at the antenna feed line. In MIMO, however, the effective SNR for each multiplexed codeword is defined after MIMO equalization; it no longer aligns with the raw field strength and therefore cannot be measured directly in the field. MIMO equalization (or often MIMO detection) is performed internally within the demodulator chipset and is therefore mostly inaccessible to field-measurement probes. Moreover, these post-processed signal-to-noise ratio (SNR) values remain distant from environmentally representative metrics, as they fail to capture channel conditions like XPD.

Hence, CNR is adopted as the target metric for ToV in MIMO systems. The CNR is obtained based on field strength measurements taken along each polarization path [23], [44], [45]. In this paper we assume equal channel power on *pol* #1 and *pol* #2, so the CNR is identical whether it is measured on *pol* #1, on *pol* #2, or averaged over both. In addition, note that the received signal on each polarization includes both the co-polarization and polarization-shifted components. The portion between them is determined by XPD. The concept of CNR captures this mixture. Based on the expression in (1), the received CNR is defined accordingly as $\frac{\mathbb{E}_{\mathbf{H}}[|h_{00}x_0|^2]+\mathbb{E}_{\mathbf{H}}[|h_{10}x_1|^2]}{\sigma_n^2} = \frac{\mathbb{E}_{\mathbf{H}}[|h_{01}x_0|^2]+\mathbb{E}_{\mathbf{H}}[|h_{11}x_1|^2]}{\sigma_n^2} = \frac{P_R}{\sigma_n^2}$. □

1) Layered MIMO Transmission: Beyond the single-layer example, this work also addresses layered MIMO, the combination of LDM and MIMO transmission. Specifically, *Layered MIMO Type A* defined in A/322:2024-09 is tackled.[9] Throughout the paper, we confine the use of the term *layered MIMO* exclusively to this *Layered MIMO Type A* configuration.

Layered MIMO overlays two independent messages in a superposition coding fashion [7]. Following ATSC 3.0 LDM terminology [46], the higher-power layer is called the *core layer (CL)*, and the lower-power layer is called the *enhanced*

[7] In this paper, a *symbol* (data or pilot) is used in the generic sense to denote a complex signal value on a single time–frequency element (one subcarrier in one OFDM symbol interval), equivalent to a *cell* in ATSC 3.0. *OFDM symbol* denotes the full OFDM symbol.

[8] This paper focuses on a symmetric case in which the two polarizations arrive with equal power. Although power imbalance could often appear in the wild, the proposed estimators still provide a useful baseline, and the framework can readily be extended to asymmetric scenarios.

[9] Layered Type A is a direct superposition that both layers use MIMO, whereas Type B combines a SISO core layer with a MIMO enhanced layer, thereby enabling backward compatibility with legacy SISO systems.

layer (EL). ATSC 3.0 systems specifically indicate CL physical-layer pipes (PLPs) by **L1D_plp_layer** $= 0$ and EL PLPs by **L1D_plp_layer** > 0. When layered MIMO is applied, the received signal is accordingly given by

$$\begin{aligned}\mathbf{y} &= \mathbf{H}\mathbf{x} + \mathbf{n} \\ &= \mathbf{H}(\mathbf{x}_c + \mathbf{x}_e) + \mathbf{n}, \end{aligned} \tag{2}$$

where $\mathbf{x}_c = [x_{c0}, x_{c1}]^T \in \mathbb{C}^{2\times 1}$ and $\mathbf{x}_e = [x_{e0}, x_{e1}]^T \in \mathbb{C}^{2\times 1}$ are the power-scaled transmit symbol vectors for CL and EL, respectively. The power split between the CL and EL is governed by the *injection level*, denoted by $\delta \in (0, 1)$, such that $\mathbf{x}_c \sim \mathcal{CN}\left(\mathbf{0}, \frac{P_R}{1+\delta}\mathbf{I}\right)$, $\mathbf{x}_e \sim \mathcal{CN}\left(\mathbf{0}, \frac{\delta P_R}{1+\delta}\mathbf{I}\right)$. In an A/322 language, the dB-scale expression $\mathtt{IL} = -10\log_{10}\delta$ is signaled by **L1D_plp_ldm_injection_level**.

Receivers interested in the CL simply use $\mathbf{y}$ in (2), treating the EL as additive noise—referred to as inter-layer interference (ILI). That is, the received CL signal $\mathbf{y}_c$ is found as $\mathbf{y}_c = \mathbf{y}$. Receivers targeting the EL, on the other hand, apply successive-interference cancellation (SIC) to remove the CL component before decoding the EL. Assuming a perfect CL cancellation, the received EL signal can then be written as

$$\begin{aligned}\mathbf{y}_e &= \mathbf{H}\mathbf{x}_e + (\mathbf{H}\mathbf{x}_c - \hat{\mathbf{H}}\hat{\mathbf{x}}_c) + \mathbf{n} \\ &\approx \mathbf{H}\mathbf{x}_e + \mathbf{n}, \end{aligned} \tag{3}$$

where $\hat{\mathbf{H}}$ and $\hat{\mathbf{x}}_c$ indicate the channel estimate and the restored CL signal, respectively [47], [48], [49]. Successful CL decoding yields $\hat{\mathbf{x}}_c = \mathbf{x}_c$. Note that, because CL decoding should be completed first for SIC, the reception requirement for the EL is typically set stricter than that for the CL [1], [20].

2) Pilot Transmission and Channel Estimation: This paper starts with Class P estimation, the baseline model that relies on the perfect CSIR, and extends further with Class E model accounting for channel estimation errors. Whereas Class P estimation can proceed directly from (1)-(3), Class E additionally unfolds the signal models as

$$\mathbf{y} = \mathbf{H}\mathbf{x} + \mathbf{n} = \underbrace{\hat{\mathbf{H}}\mathbf{x}}_{\text{desired}} + \underbrace{\tilde{\mathbf{H}}\mathbf{x} + \mathbf{n}}_{\text{effective noise}}, \tag{4}$$

$$\mathbf{y}_c = \underbrace{\hat{\mathbf{H}}\mathbf{x}_c}_{\text{desired}} + \underbrace{\tilde{\mathbf{H}}\mathbf{x}_c + \mathbf{H}\mathbf{x}_e + \mathbf{n}}_{\text{effective noise}}, \tag{5}$$

$$\mathbf{y}_e = \underbrace{\hat{\mathbf{H}}\mathbf{x}_e}_{\text{desired}} + \underbrace{\tilde{\mathbf{H}}\mathbf{x}_c + \tilde{\mathbf{H}}\mathbf{x}_e + \mathbf{n}}_{\text{effective noise}}, \tag{6}$$

where $\hat{\mathbf{H}}$ and $\tilde{\mathbf{H}} = \mathbf{H} - \hat{\mathbf{H}}$ stand for the channel estimate at the receiver and its estimation error from the true $\mathbf{H}$, respectively [50]. When Class E is considered, pilot signals can contribute the received signal strength P_R, we specify the data signal power by $\mathbf{x} \sim \mathcal{CN}(\mathbf{0}, P_d\mathbf{I})$, $\mathbf{x}_c \sim \mathcal{CN}\left(\mathbf{0}, \frac{P_d}{1+\delta}\mathbf{I}\right)$, and $\mathbf{x}_e \sim \mathcal{CN}\left(\mathbf{0}, \frac{\delta P_d}{1+\delta}\mathbf{I}\right)$ with notation P_d. Note here that the effective signal quality can deteriorate further, depending on channel estimation accuracy.

Class E procedures employ a linear MMSE (LMMSE) channel estimator to model $\hat{\mathbf{H}}$ and $\tilde{\mathbf{H}}$, thereby yielding a tractable, standard theoretical framework. As in conventional wireless systems, the process is pilot-driven, and the pilot topology is simplified as follows.

The channel follows a block-fading model: The state remains constant within a fading block, and one pilot symbol matrix is assumed to serve a single block. Regarding the cardinality of 2×2 MIMO, the LMMSE filter uses a two-symbol window; that is, two adjacent pilot cells belong to the same block. Preserving orthogonality, the pilot vectors are given by $\mathbf{p}_1 = [p, 0]^T$ and $\mathbf{p}_2 = [0, p]^T$ for $^\exists p \in \mathbb{C}$, where the first entry is the *pol* #1 component and the second is the *pol* #2 component. Transmitted in successive pilot instants, $\mathbf{p}_1$ and $\mathbf{p}_2$ form a space-time signal matrix

$$\mathbf{P} = p\mathbf{I} = \begin{bmatrix} p & 0 \\ 0 & p \end{bmatrix}. \tag{7}$$

Note that the pilot power $P_p = |p|^2$ is determined as relative to the data signal power P_d by $P_p = 2A_{\mathrm{SP}}^2 P_d$, where $A_{\mathrm{SP}} = 10^{\frac{F_{\mathrm{PB}}}{20}}$ is an amplitude gain introduced by pilot boosting[10] of F_{PB} dB. P_p and P_d satisfy $P_p = 2A_{\mathrm{SP}}^2 \kappa_d P_R$ and $P_d = \kappa_d P_R$, where

$$\kappa_d = \frac{1}{1 - \frac{1}{D_X D_Y} + \frac{A_{\mathrm{SP}}^2}{D_X D_Y}} \tag{8}$$

represents the amount of data signal power reduction due to pilot boosting [51]. D_X and D_Y here denote the frequency- and time-domain separations of adjacent pilots, respectively, in an OFDM cell unit. In ATSC 3.0 systems, D_X and D_Y are signaled by the scattered pilot pattern indicator **L1B_first_sub_scattered_pilot_pattern** or **L1D_scattered_pilot_pattern**. We assume that D_X and D_Y are chosen dense enough to ensure block-fading within an inter-pilot duration.

B. Channel Models

This work considers three channel types: AWGN, Rayleigh (RL), and Rician (RC). Each model imposes different statistical properties on $\mathbf{H}$.

AWGN channel represents a situation where the channel consists solely of line-of-sight (LoS) paths; RL channel depicts the converse where the channel consists solely of non-LoS (NLoS) scatters. RC channel represents the case having both LoS and NLoS components, where the power ratio between those is characterized by Rician K-factor.

Each corresponding realization of $\mathbf{H}$ is described in Table I, where:

- $\rho_L \in (\frac{1}{2}, 1]$ identifies the power portion of co- and cross-polarization components in the LoS part of MIMO channel. This value is determined by χ_L^{dB};
- $\rho_N \in (\frac{1}{2}, 1]$ identifies the power portion of co- and cross-polarization components in the NLoS part of MIMO channel. This value is determined by χ_N^{dB};
- g_{00}, g_{10}, g_{01}, g_{11} denote the normalized random fading gain at each MIMO channel entry, which are i.i.d. random variables conforming to $\mathcal{CN}(0, 1)$;
- K is the Rician K-factor.

Shortly, $\mathbf{H} = \mathbf{H}_\mu$ holds when $^\exists\mu \in \{\mathtt{AWGN}, \mathtt{RL}, \mathtt{RC}\}$ is determined.

[10] See **L1D_scattered_pilot_boost** in A/322 and the lookup tables related.

TABLE I
CHANNEL MODEL DESCRIPTION

Channel Model	Formulaic Description
AWGN (Full LoS)	$\mathbf{H}_{\text{AWGN}} = \begin{bmatrix} \sqrt{\rho_L} & \sqrt{1-\rho_L} \\ \sqrt{1-\rho_L} & \sqrt{\rho_L} \end{bmatrix}$
RL	$\mathbf{H}_{\text{RL}} = \begin{bmatrix} \sqrt{\rho_N} g_{00} & \sqrt{1-\rho_N} g_{10} \\ \sqrt{1-\rho_N} g_{01} & \sqrt{\rho_N} g_{11} \end{bmatrix}$
RC	$\mathbf{H}_{\text{RC}} = \sqrt{\frac{K}{1+K}} \mathbf{H}_{\text{AWGN}} + \sqrt{\frac{1}{1+K}} \mathbf{H}_{\text{RL}}$

Note that $g_{ij\in\{00,10,01,11\}}$s are the only random variables presenting randomness of the channel. That means, $\mathbf{H}_{\text{AWGN}}$ is truly deterministic, while $\mathbf{H}_{\text{RL}}$ and $\mathbf{H}_{\text{RC}}$ involve randomness such that $\text{vec}(\mathbf{H}_{\text{RL}}) \sim \mathcal{CN}(\mathbf{0}, \text{diag}(\rho_N, 1-\rho_N, 1-\rho_N, \rho_N))$, $\text{vec}(\mathbf{H}_{\text{RC}}) \sim \mathcal{CN}\left(\sqrt{\frac{K}{1+K}}\text{vec}(\mathbf{H}_{\text{AWGN}}), \sqrt{\frac{1}{1+K}}\text{diag}(\rho_N, 1-\rho_N, 1-\rho_N, \rho_N)\right)$. NLoS components are designed as random, whereas the LoS components remain deterministic.

ρ_L and ρ_N, identifying the power of each element, are determined by the channel XPDs on LoS/NLoS part. XPD is generically defined as

$$\text{XPD} = \frac{\text{Co-polarized signal power}}{\text{Polarization-shifted signal power}}$$

measured within each received polarization wave. We specify the term *channel XPD* as the XPD measured from the input to the output of MIMO channel, thereby including the combined effects of fading and antenna isolation (see Section VII for details). When both LoS and NLoS components are present, separate channel XPDs are defined, as χ_L^{dB} and χ_N^{dB}. The relationship among ρ_L, χ_L^{dB}, ρ_N, and χ_N^{dB} are described as

$$\rho_L = \frac{10^{\frac{\chi_L^{\text{dB}}}{10}}}{1+10^{\frac{\chi_L^{\text{dB}}}{10}}}, \quad \rho_N = \frac{10^{\frac{\chi_N^{\text{dB}}}{10}}}{1+10^{\frac{\chi_N^{\text{dB}}}{10}}}. \tag{9}$$

For convenience we collect these parameters in the channel XPD configuration identifier $\Theta_{\text{XPD}} \triangleq (\chi_L^{\text{dB}}, \chi_N^{\text{dB}})$. Each term is defined only when available: $\Theta_{\text{XPD}} = \chi_L^{\text{dB}}$ for $\mathbf{H}_{\text{AWGN}}$, $\Theta_{\text{XPD}} = \chi_N^{\text{dB}}$ for $\mathbf{H}_{\text{RL}}$, and $\Theta_{\text{XPD}} \triangleq (\chi_L^{\text{dB}}, \chi_N^{\text{dB}})$ for $\mathbf{H}_{\text{RC}}$.

Notably, the proposed ToV estimators incorporate preset offset functions to tackle the analytical intractability of the objective functions (see Section V). The coefficients of these offset functions are precomputed offline by matching the approximative equivalents to their target objectives. Accordingly, the present methods, with the given offsets, support a finite set of Θ_{XPD} values listed in Table II, but can be readily extended to other cases once the corresponding offsets are computed. For intermediate XPD values currently not listed in Table II, users may interpolate the estimation results (or precomputed offset coefficients) between neighboring Θ_{XPD} points. As a simpler practical alternative, users may use the results corresponding to the nearest tabulated Θ_{XPD} value as an approximation. Furthermore, with field use in mind, we primarily reference the standard channel models widely adopted in the broadcasting industry, namely AWGN, RL20 (DVB-P1), and RC20 (DVB-F1). Thus, a Rician K-factor of $K = 10$ is used for the Rician condition, in accordance with the RC20 profile.

C. Organization, Structure of the Estimator Program

Briefly, the proposed ToV estimators, hereafter called *ToV Estimators*, operate as follows: Given the SISO ToV measurement τ_{S} as input, *ToV Estimators* convert it into the corresponding MIMO ToV estimate τ_{M}. The process also requires a set of system and channel parameters as input, depending on the target scenario:

- Always required: Estimator class (Class P/E), use of LDM and the target layer (single-layer, CL, or EL), μ, and Θ_{XPD}
- Required only for layered MIMO cases:δ
- Required only for Class E estimation: F_{PB}, D_X, and D_Y

ToV Estimators have six operating modes characterized by the CSIR assumption and transmission layer configuration. Primarily, the methods are classified into two modes: Class P and Class E below.

- Class P: Perfect CSIR assumed.
- Class E: Channel estimation errors accounted.

The operation mode is further subdivided according to the transmission layer configuration as follows:

- Single-layer (SL) mode: LDM is not applied (non-layered MIMO).
- CL-target mode: Layered MIMO is applied and the ToV for CL is to be estimated.
- EL-target mode: Layered MIMO is applied and the ToV for EL is to be estimated.

§ *Remark: Reference measurements* τ_{S}

To be emphasized, $\boldsymbol{\tau_{\text{S}}}$ **must be taken only from SISO ToV data measured under unfaded (AWGN) conditions.** For instance, Annex A of A/327 [1] lists SISO ToVs for four different channel conditions (AWGN, RC20, RL20, and TU-6) in Tables A.3.2–A.3.6. Among these, only Table A.3.2 obtained with the AWGN channel can be used for τ_{S}. *ToV Estimators* are built as wholly responsible for fading effects, leaving τ_{S} to serve as an uncontaminated ground truth.

As a brief example, Table III lists a subset of the SISO ToV data excerpted from A/327. Each ToV is specified for a particular modulation profile, including a unique combination of ModCod. A/327 also provides measurements obtained under several test conditions, such as BICM-only simulations, end-to-end link-level simulations, hardware-based laboratory tests, and over-the-air field trials. An appropriate data set may be selected depending on the user's intent. For τ_{S} in this work, we recommend using the link-level simulation results (labelled 'Simulation' in A/327 and in Table III) or the laboratory test results (labelled 'Lab Test').

Such τ_{S} values can be regarded as perfect-CSIR observations because fading has been omitted. That is, Class E procedure deals solely with the CSIR errors at the MIMO receiver, since CSIR error-free τ_{S} is used as reference. In addition, τ_{S} refers to the measurement obtained without pilot boosting.

The QEF criteria applied to the estimation result are consistent with those used to measure the rationale SISO performance data. The A/327 data were measured at bit error

TABLE II
CHANNEL XPD CONFIGURATIONS SUPPORTED IN ESTIMATION MODELS

Channel Model	XPD Configuration Θ_{XPD}	
	XPD in LoS components: χ_L^{dB}	XPD in LoS components: χ_N^{dB}
AWGN	Any values are applicable if $\chi_L^{\text{dB}} \geq 0$ dB	Not Defined (NLoS signals absent)
Rayleigh	Not Defined (LoS signals absent)	20 dB
		10 dB
		5 dB
		0 dB
Rician ($K = 10$)	20 dB	20 dB
		10 dB
		5 dB
		0 dB
	10 dB	10 dB
		5 dB
		0 dB

TABLE III
SEVERAL EXAMPLES OF SISO TOV VALUES EXTRACTED FROM A/327, AWGN CHANNEL RESULTS [DB]

Constellation	Code Length	Meas. Setup	Code Rate		
			2/15	8/15	12/15
QPSK	Long (64,800 bits)	BICM Sim.	-6.23	1.15	4.48
		Simulation	-6.09	1.32	4.61
		Lab Test	-4.01	2.00	5.10
		Field Test	-3.88	2.18	5.26
	Short (16,200 bits)	BICM	-5.56	1.37	4.70
		Simulation	-5.49	1.51	4.82
		Lab Test	-4.23	2.10	5.10
		Field Test	-4.07	2.32	5.27
64 NUC	Long (64,800 bits)	BICM	-0.27	10.30	15.56
		Simulation	-0.18	10.52	15.72
		Lab Test	0.50	11.30	16.30
		Field Test	0.65	11.42	16.59

rate (BER) = 10^{-6} (i.e., frame error rate (FER) = 10^{-4}), and the MIMO ToV estimates deduced therefrom are interpreted to promise the same error performance. Note that the estimation model may also use other reference datasets (instead of A/327 Annex A) measured at different target error rates. The guaranteed error performance should follow the referenced criteria thereof.

To avoid any confusion, note also that τ_{S} is always taken from single-layer (non-LDM) measurements. More directly, the SL reference τ_{S} must be used even when estimating the τ_{M} for CL or EL in layered MIMO setups. For convenience, let $\tau_{\text{M}}^{\text{CL}}$ and $\tau_{\text{M}}^{\text{EL}}$ denote the τ_{M}s for CL and EL, respectively. One should again remind here that each estimated τ_{M} is tied to the ModCod setting of its underlying SISO SL reference. In precise terms, it can be said: $\tau_{\text{M}}^{\text{CL}}$ is the total CNR required to decode the CL when the CL uses the same ModCod as the SL SISO test obtained τ_{S}; $\tau_{\text{M}}^{\text{EL}}$ is the total CNR required to decode the EL when the EL uses the same ModCod scheme tied with τ_{S}. □

III. RESULTS PART I: PERFECT CSIR CASE (CLASS P)

This section presents the closed-form results for Class P *ToV Estimator* and its workflow. Class P assumes perfect CSIR and thus constitutes a theoretical bound under an idealized receiver. Despite this premise, the Class P procedure is the simplest to apply and is broadly useful in practice. Results for SL transmission appear in Section III-A; Section III-B extends the results to layered MIMO.

A. SL (Non-LDM) Scenarios

The SL-case Class P procedure forms the baseline for all *ToV Estimator* variants presented. The SL Class P estimator is summarized in *Result 1* below, which unifies the AWGN, RL, and RC cases under a single parameterized framework.

§ *Result 1 (Class P estimates for SL transmission):* As long as LDM is unused, the generalized formula for Class P estimation is described as

$$\tau_{\text{M}} = \zeta \times 10^{\frac{f_{\text{co}}^{\mu}(\zeta_{\text{dB}}|\Theta_{\text{XPD}})}{10}}, \tag{10}$$

whose dB-scale expression, which practitioners are more used to, is given by

$$\begin{aligned} \text{Required CNR [dB]} &= 10\log_{10}\tau_{\text{M}} \\ &= 10\log_{10}\zeta + f_{\text{co}}^{\mu}(\zeta_{\text{dB}}|\Theta_{\text{XPD}}). \end{aligned} \tag{11}$$

This is composed of an intermediate estimate

$$\zeta = \frac{-1 + \sqrt{1 + \Omega_{\mu}(\mathcal{E}_R - 1)}}{\Omega_{\mu}} \tag{12}$$

and a correction offset function $f_{\text{co}}^{\mu}(\zeta_{\text{dB}}|\Theta_{\text{XPD}})$, where $\zeta_{\text{dB}} = 10\log_{10}\zeta$. Note that each μ realization (i.e., AWGN, RL, or RC) has a unique $f_{\text{co}}^{\mu}(\zeta_{\text{dB}}|\Theta_{\text{XPD}})$. Sections III-A.1, III-A.2, and III-A.3 below detail their respective definitions.

The parameters $\mathcal{E}_R$ and Ω_{μ} are specified as

$$\mathcal{E}_R = 1 + 2\tau_{\text{S}} + \tau_{\text{S}}^2 \tag{13}$$

and

$$\Omega_{\mu} = \begin{cases} \Omega_{\text{AWGN}} & \mu = \texttt{AWGN} \\ \Omega_{\text{RL}} & \mu = \texttt{RL} \\ \Omega_{\text{RC}} & \mu = \texttt{RC} \end{cases} \tag{14}$$

given as dependent on τ_{S} and μ, respectively. Each realization of Ω_{μ} is a scalar coefficient solely determined by XPD values; and is quantified in Sections III-A.1, III-A.2, and III-A.3.

The estimation procedure computing τ_{M} unfolds as Algorithm 1.

TABLE IV

COEFFICIENTS OF $f_{\text{co}}^{\text{RL}}(\zeta_{\text{dB}} \mid \Theta_{\text{XPD}})$ W.R.T. XPD LEVELS

XPD Configuration χ_N^{dB}	c_5	c_4	c_3	c_2	c_1	c_0
20 dB	-1.237×10^{-7}	1.156×10^{-5}	-3.366×10^{-4}	8.187×10^{-4}	1.17×10^{-1}	0.9813
10 dB	-1.263×10^{-7}	1.225×10^{-5}	-3.841×10^{-4}	2.000×10^{-3}	1.08×10^{-1}	0.8518
5 dB	-9.448×10^{-8}	1.005×10^{-5}	-3.544×10^{-4}	2.814×10^{-3}	8.911×10^{-2}	0.6548
0 dB	-5.598×10^{-8}	7.061×10^{-6}	-2.891×10^{-4}	2.997×10^{-3}	6.902×10^{-2}	0.4957

Algorithm 1 Class P Procedure in SL Scenarios

Input: τ_{S}, μ, and Θ_{XPD}.

procedure CLASS P, SL
  Initialization Compute $\mathcal{E}_R$ and Ω_μ.
  Step 1: Compute ζ using (12).
  Step 2: Obtain τ_{M} by applying $f_{\text{co}}^{\mu}(\zeta_{\text{dB}}|\Theta_{\text{XPD}})$.
    Use $\zeta_{\text{dB}} = 10\log_{10}\zeta$.
end procedure
return τ_{M}.

TABLE V

VALUES OF $f_{\text{sat}}^{\text{RL}}$ W.R.T. XPD LEVELS

XPD Configuration χ_N^{dB}	$f_{\text{sat}}^{\text{RL}}$ [dB]
20 dB	2.50
10 dB	2.41
5 dB	2.14
0 dB	1.83

1) AWGN Channel (Full-LoS): $\Theta_{\text{XPD}} = \chi_L^{\text{dB}}$ holds when $\mu = \texttt{AWGN}$ since only LoS components are present; the NLoS parameters ρ_N, χ_N^{dB} are undefined.

Given ρ_L by (9), the parameter Ω_μ is specified as

$$\Omega_{\text{AWGN}} = (2\rho_L - 1)^2, \tag{15}$$

and $f_{\text{co}}^{\mu}(\zeta_{\text{dB}}|\Theta_{\text{XPD}}) = 0$ always holds regardless of any ζ_{dB} and Θ_{XPD}. Shortly,

$$\tau_{\text{M}} = \begin{cases} \frac{-1+\sqrt{1+(2\rho_L-1)^2(2\tau_{\text{S}}+\tau_{\text{S}}^2)}}{(2\rho_L-1)^2} & \rho_L > \frac{1}{2}\ (\chi_L^{\text{dB}} > 0) \\ \tau_{\text{S}} + \frac{\tau_{\text{S}}^2}{2} & \rho_L = \frac{1}{2}\ (\chi_L^{\text{dB}} = 0) \end{cases} \tag{16}$$

holds for the AWGN channel case.

Note that, under AWGN conditions, this model permits any real-valued ρ_L in the range of $\frac{1}{2} < \rho_L \leq 1$. This means that any $\chi_L^{\text{dB}} \geq 0$ is supported.

2) Rayleigh (RL) Channel: $\Theta_{\text{XPD}} = \chi_N^{\text{dB}}$ holds when $\mu = \texttt{RL}$ since only NLoS components are present; the LoS parameters ρ_L, χ_L^{dB} are undefined.

Given ρ_N by (9), the parameter Ω_μ is specified as

$$\Omega_{\text{RL}} = \rho_N^2 + (1 - \rho_N)^2. \tag{17}$$

When conditioned on RL channel, a correction offset function

$$f_{\text{co}}^{\text{RL}}(\zeta_{\text{dB}}|\Theta_{\text{XPD}}) = \begin{cases} \sum_{k=0}^{5} c_k \times (\zeta_{\text{dB}})^k & \zeta_{\text{dB}} < 30 \\ f_{\text{sat}}^{\text{RL}} & \zeta_{\text{dB}} \geq 30 \end{cases} \tag{18}$$

applies to (10) (see **Step 2** in Algorithm 1). The coefficients $c_{k\in\{0,1,\cdots 5\}}$ constructing $f_{\text{co}}^{\text{RL}}(\cdot)$ refer to Table IV. Note that these coefficient values are also specific to χ_N^{dB}.

(18) relates that $f_{\text{co}}^{\text{RL}}(\cdot)$ is saturated by $f_{\text{sat}}^{\text{RL}}$ when $\zeta_{\text{dB}} \geq 30$ dB. Table V specifies this value $f_{\text{sat}}^{\text{RL}}$ according to χ_N^{dB}.

3) Rician (RC) Channel: When $\mu = \texttt{RC}$, both χ_L^{dB} and χ_N^{dB} are defined; accordingly, the XPD condition is the pair $\Theta_{\text{XPD}} = (\chi_L^{\text{dB}}, \chi_N^{\text{dB}})$.

Given ρ_L and ρ_N by (9), the parameter Ω_μ is specified as

$$\Omega_{\text{RC}} = \left(\frac{\rho_L K}{1+K} + \frac{\rho_N}{1+K}\right)^2 + \left(\frac{(1-\rho_L)K}{1+K} + \frac{(1-\rho_N)}{1+K}\right)^2 - \frac{2\rho_L(1-\rho_L)K^2}{(1+K)^2}, \tag{19}$$

and the correction offset function

$$f_{\text{co}}^{\text{RC}}(\zeta_{\text{dB}}|\Theta_{\text{XPD}}) = \begin{cases} \sum_{k=0}^{5} c_k \times (\zeta_{\text{dB}})^k & \zeta_{\text{dB}} < 30 \\ f_{\text{sat}}^{\text{RC}} & \zeta_{\text{dB}} \geq 30 \end{cases} \tag{20}$$

applies to (10) (see **Step 2** in Algorithm 1). The coefficients $c_{k\in\{0,1,\cdots,5\}}$ in $f_{\text{co}}^{\text{RC}}(\cdot)$ are enumerated in Table VI. Note that these coefficient values are also specific to the pair $(\chi_L^{\text{dB}}, \chi_N^{\text{dB}})$.

Note also that $f_{\text{co}}^{\text{RC}}(\cdot)$ is saturated by $f_{\text{sat}}^{\text{RC}}$ when $\zeta_{\text{dB}} \geq 30$ dB. Table VII specifies this value $f_{\text{sat}}^{\text{RC}}$ according to $(\chi_L^{\text{dB}}, \chi_N^{\text{dB}})$.

§ *Corollary 1.1: Asymptote of the SL mode Class P estimate*

Asymptote of (10) at $\tau_{\text{S}} \gg 1$ provides a convenient, coarse estimate

$$\tau_{\text{M}} \underset{\tau_{\text{S}}\gg 1}{\longrightarrow} \frac{\tau_{\text{S}}}{\sqrt{\Omega_\mu}} \times 10^{\frac{f_{\text{sat}}^{\mu}}{10}}, \tag{21}$$

which leads to ToV [dB] $\to 10\log_{10}\frac{\tau_{\text{S}}}{\sqrt{\Omega_\mu}} + f_{\text{sat}}^{\mu}$. Note that this asymptote applies to $\mu = \texttt{RL}$ and $\texttt{RC}$, while the $\mu = \texttt{AWGN}$ case directly finds $\tau_{\text{M}} \to \frac{\tau_{\text{S}}}{\sqrt{\Omega_\mu}}$.

B. LDM Scenarios (Layered MIMO Type A)

This section presents Class P procedures for layered MIMO transmission. Accordingly, the estimate τ_{M} is identified for each LDM layer in the following subsections.

1) CL-Target Mode: As mentioned in Section II-C, the CL-target mode yields the total CNR required to decode the CL in layered MIMO signals. The proposed method for this mode is summarized in *Result 2*, covering all μ cases. For clarity, we explicitly denote the ToV estimate in this mode (otherwise generically written as τ_{M}) by $\tau_{\text{M}}^{\text{CL}}$.

§ *Result 2 (Class P estimate, CL in Layered MIMO Type A):* The Class P estimation in this mode is attributed to

$$\tau_{\text{M}}^{\text{CL}} = \frac{\hat{\zeta}_{\text{CL}}}{1 - \Delta_{\text{LDM}} - \Delta_{\text{LDM}}\hat{\zeta}_{\text{CL}}}, \tag{22}$$

where the auxiliary variable $\hat{\zeta}_{\text{CL}}$ is expressed as

$$\hat{\zeta}_{\text{CL}} = \zeta_{\text{CL}} \times 10^{\frac{f_{\text{co}}^{\mu}(\zeta_{\text{CL}}^{\text{dB}}|\Theta_{\text{XPD}})}{10}}, \tag{23}$$

TABLE VI
COEFFICIENTS OF $f_{\text{co}}^{\text{RC}}(\zeta_{\text{dB}}|\Theta_{\text{XPD}})$ W.R.T. XPD LEVELS

XPD Configuration Θ_{XPD}		Coefficients					
χ_L^{dB}	χ_N^{dB}	c_5	c_4	c_3	c_2	c_1	c_0
20 dB	20 dB	-2.504×10^{-8}	2.234×10^{-6}	-5.701×10^{-5}	-1.261×10^{-4}	2.266×10^{-2}	0.1916
	10 dB	-1.961×10^{-8}	1.782×10^{-6}	-4.566×10^{-5}	-1.64×10^{-4}	2.088×10^{-2}	0.1766
	5 dB	-1.784×10^{-8}	1.625×10^{-6}	-4.239×10^{-5}	-9.539×10^{-5}	1.764×10^{-2}	0.1478
	0 dB	-1.073×10^{-8}	9.887×10^{-7}	-2.627×10^{-5}	-6.453×10^{-5}	1.193×10^{-2}	9.908×10^{-2}
10 dB	10 dB	-3.442×10^{-8}	3.416×10^{-6}	-1.072×10^{-4}	5.958×10^{-4}	2.508×10^{-2}	0.1751
	5 dB	-2.896×10^{-8}	2.944×10^{-6}	-9.511×10^{-5}	5.922×10^{-4}	2.127×10^{-2}	0.1466
	0 dB	-1.965×10^{-8}	2.109×10^{-6}	-7.294×10^{-5}	5.714×10^{-4}	1.458×10^{-2}	9.731×10^{-2}

TABLE VII
VALUES OF $f_{\text{sat}}^{\text{RC}}$ W.R.T. XPD LEVELS

XPD Configuration Θ_{XPD}		$f_{\text{sat}}^{\text{RC}}$ [dB]
χ_L^{dB}	χ_N^{dB}	
20 dB	20 dB	0.42
	10 dB	0.39
	5 dB	0.33
	0 dB	0.22
10 dB	10 dB	0.50
	5 dB	0.43
	0 dB	0.31

and where

$$\Delta_{\text{LDM}} = \frac{\delta}{1+\delta}. \tag{24}$$

represents the effective EL power portion. As noted earlier, $\delta \in (0,1)$ is a linear-scale variable, whereas specification language of A/322 often uses $\mathtt{IL} = -10\log_{10}\delta$ signaled by **L1D_plp_ldm_injection_level**.

The parameter ζ_{CL} in (23) is defined as

$$\zeta_{\text{CL}} = \frac{(1-\Delta_{\text{LDM}})\zeta_c}{1+\Delta_{\text{LDM}}\zeta_c} \tag{25}$$

and the same $f_{\text{co}}^{\mu}(\cdot)$ as in Section III-A is applied while holding $\zeta_{\text{CL}}^{\text{dB}} = 10\log_{10}\zeta_{\text{CL}}$ as input. (25) can be viewed as a Möbius transform of ζ_c, where the parameter ζ_c defining ζ_{CL} is given by (26), as shown at the bottom of the page. $\mathcal{E}_R$ and Ω_μ in (26) follow the definitions given in the previous section.

The estimation procedure computing $\tau_{\text{M}}^{\text{CL}}$ is summarized in Algorithm 2. Expediting the process, $\tau_{\text{M}}^{\text{CL}}$ reduces to $\tau_{\text{M}}^{\text{CL}} = \zeta_c$ when $\mu = \mathtt{AWGN}$. Note also that the value τ_{S} corresponds to the measurement obtained without applying LDM.

2) EL-Target Mode: The EL-target mode yields the total CNR required to decode the EL in layered MIMO signals. Likewise, the ToV estimate in this mode is denoted by $\tau_{\text{M}}^{\text{EL}}$, and the proposed method for this mode is summarized in *Result 3*.

§ *Result 3 (Class P estimate, EL in Layered MIMO Type A):* The Class P estimation in this mode is expressed as

$$\tau_{\text{M}}^{\text{EL}} = \frac{\zeta}{\Delta_{\text{LDM}}} \times 10^{\frac{f_{\text{co}}^{\mu}(\zeta_{\text{dB}}|\Theta_{\text{XPD}})}{10}}$$

$$= \frac{-1+\sqrt{1+\Omega_\mu(\mathcal{E}_R-1)}}{\Omega_\mu\Delta_{\text{LDM}}} \times 10^{\frac{f_{\text{co}}^{\mu}(\zeta_{\text{dB}}|\Theta_{\text{XPD}})}{10}} \tag{27}$$

where the related parameters ζ, Δ_{LDM}, and $\mathcal{E}_R$ are given by (12), (24), and (13), respectively. The same $f_{\text{co}}^{\mu}(\cdot)$ as in Section III-A is applied. The estimation proceeds in the same manner as that described in Section III-A, with the additional division by Δ_{LDM}. This procedure is summarized in Algorithm 3. Again, τ_{S} corresponds to the measurement obtained without applying LDM.

IV. RESULTS PART II: ESTIMATED CSIR CASE (CLASS E)

The Class E procedure is an extension of Class P, specifically designed to capture the impact of channel estimation errors. CSI errors are embodied through an actual pilot-based channel estimation process; this also provides a means to scale system performance according to pilot boosting. Class E procedure specifically employs an LMMSE channel estimation, which renders it a theoretical reference model. Accordingly, system performance in commercial receivers may partly vary depending on the channel estimation schemes implemented.

For the Class E procedure, the pilot topology and related definitions are given in Section II-A.2. In particular, the definitions of F_{PB}, A_{SP}, D_X, D_Y, and κ_d are provided therein. It should be noted that the referenced τ_{S} values correspond to measurements obtained without applying pilot boosting.

A. SL Scenarios

§ *Result 4 (Class E estimates for SL transmission):* When the transmission is configured in SL mode, the Class E *ToV estimate* is given as follows.

1) AWGN Channel (Result 4-1): When $\mu = \mathtt{AWGN}$, channel estimation errors are absent. In this case, the Class E estimate reduces to the Class P estimation of Section III-A.1 unless pilot boosting is applied. Once the Class E-version of $f_{\text{co}}^{\mu}(\cdot)$ is defined as $f_{\text{co}}^{\mu|\text{CE}}(\cdot)$, we can write $f_{\text{co}}^{\text{AWGN}|\text{CE}}(\zeta_{\text{dB}}|\Theta_{\text{XPD}}) = 0$.

When pilot boosting applies, the result becomes

$$\tau_{\text{M}} = \frac{\zeta}{\kappa_d}, \tag{28}$$

where ζ and κ_d are defined in (12) and (8), respectively.

$$\zeta_c = \frac{\mathcal{E}_R\Delta_{\text{LDM}} - 1 + \sqrt{(\mathcal{E}_R\Delta_{\text{LDM}}-1)^2 + \Omega_\mu(1-\mathcal{E}_R\Delta_{\text{LDM}}^2)(\mathcal{E}_R-1)}}{\Omega_\mu(1-\mathcal{E}_R\Delta_{\text{LDM}}^2)} \tag{26}$$

TABLE VIII
COEFFICIENTS OF $f_{\text{co}}^{\text{RL|CE}}(\zeta_{\text{dB}} \mid \Theta_{\text{XPD}})$ W.R.T. XPD LEVELS

XPD Configuration χ_N^{dB}	c_5	c_4	c_3	c_2	c_1	c_0
20 dB	-1.761×10^{-7}	1.571×10^{-5}	-4.391×10^{-4}	1.377×10^{-3}	1.255×10^{-1}	0.9056
10 dB	-1.6×10^{-7}	1.485×10^{-5}	-4.469×10^{-4}	2.345×10^{-3}	1.149×10^{-1}	0.7823
5 dB	-1.072×10^{-7}	1.141×10^{-5}	-4.008×10^{-4}	3.255×10^{-3}	9.319×10^{-2}	0.5874
0 dB	-6.628×10^{-8}	8.22×10^{-6}	-3.313×10^{-4}	3.483×10^{-3}	7.17×10^{-2}	0.4319

Algorithm 2 Class P Procedure for CL (layered MIMO)

Input: Given τ_{S}, μ, Θ_{XPD}, and δ.

```
procedure CLASS P, LDM CL
    Initialization Compute 𝓔_R, Ω_μ, and Δ_LDM.
    Step 1: Compute ζ_c using (26).
    Step 2:
    if μ = AWGN then
        τ_M^CL ← ζ_c                                   ▷ f_co^AWGN(·) = 0
        end procedure and return τ_M^CL.
    else
        Convert ζ into ζ_CL using (25).
        Proceed to Step 3
    end if
    Step 3: Obtain ζ̂_CL via (23).
            ▷ Apply (18) if μ = RL, and (20) if μ = RC.
            ▷ Use ζ_CL^dB = 10 log10 ζ_CL.
    Step 4: Obtain τ_M^CL from (22).
end procedure
return τ_M^CL.
```

Algorithm 3 Class P Procedure for EL (layered MIMO)

Input: Given τ_{S}, μ, Θ_{XPD}, and δ.

```
procedure CLASS P, LDM EL
    Initialization Compute 𝓔_R, Ω_μ, and Δ_LDM.
    Step 1: Compute ζ using (12).
    Step 2: Obtain ζ_EL via (27).
            ▷ By applying f_co^μ(ζ_dB|Θ_XPD) to ζ/Δ_LDM.
end procedure
return τ_M^EL.
```

2) RL Channel (Result 4-2): When $\mu = \texttt{RL}$, τ_{M} is determined by

$$\tau_{\text{M}} = \frac{(1 + A_{\text{SP}}^2)\hat{\zeta} + \sqrt{\left(1 + A_{\text{SP}}^2\right)^2 \hat{\zeta}^2 + 4A_{\text{SP}}^2 \hat{\zeta}}}{2A_{\text{SP}}^2 \kappa_d} \tag{29}$$

where A_{SP} and κ_d are defined in Section II-A.2 (see (8)), and

$$\hat{\zeta} = \zeta \times 10^{\frac{f_{\text{co}}^{\text{RL|CE}}(\zeta_{\text{dB}}|\Theta_{\text{XPD}})}{10}} \tag{30}$$

with ζ following (12). If pilot boosting is not applied, (29) simplifies to $\tau_{\text{M}} = \hat{\zeta} + \sqrt{\hat{\zeta}^2 + \hat{\zeta}}$. The intermediate estimate $\hat{\zeta}$ incorporates the correction offset function

$$f_{\text{co}}^{\text{RL|CE}}(\zeta_{\text{dB}}|\Theta_{\text{XPD}}) = \begin{cases} \sum_{k=0}^{5} c_k \times (\zeta_{\text{dB}})^k & \zeta_{\text{dB}} < 30 \\ f_{\text{sat}}^{\text{RL}} & \zeta_{\text{dB}} \geq 30 \end{cases} \tag{31}$$

where $\zeta_{\text{dB}} = 10 \log_{10} \zeta$ and $\mathcal{E}_R$ is determined from τ_{S} by (13). The coefficients $c_{k \in 0,1,\cdots,5}$ are listed in Table VIII.

Algorithm 4 Class E Procedure: SL Mode

Input: τ_{S}, μ, Θ_{XPD}, F_{PB}, D_X, D_Y.

```
procedure CLASS E, SL
    Initialization: Compute 𝓔_R, Ω_μ, A_SP, and κ_d.
    Step 1: Compute ζ using (12).
    Step 2:
    if μ = AWGN then
        Obtain τ_M using (28).
        end procedure.
    else
        Obtain ζ̂ by applying f_co^{μ|CE}(ζ_dB|Θ_XPD).
        Proceed to Step 3.
    end if
    Step 3: Convert ζ̂ into τ_M.
            ▷ Use (29) if μ = RL, and (33) if μ = RC.
end procedure
return τ_M.
```

Note that this $f_{\text{co}}^{\text{RL|CE}}(\cdot)$ differs from the $f_{\text{co}}^{\text{RL}}(\cdot)$ shown in Section III-A.2.

However, (31) saturates at the same level $f_{\text{sat}}^{\text{RL}}$ when $\zeta_{\text{dB}} \geq 30$ dB. See Table V listing the values $f_{\text{sat}}^{\text{RL}}$ with respect to χ_N^{dB}.

In summary, the Class E method involves one additional step compared to the Class P process, namely the extraction of (29) from (30). The estimation procedure is summarized in Algorithm 4.

§ *Corollary 4.1: Asymptote of the SL mode Class E estimate*

Similarly to *Corollary 1.1*, an accessible rule-of-thumb estimate can be obtained by observing the asymptote of (29) at $\tau_{\text{S}} \gg 1$. This asymptotic, coarse estimate is a scaled version of (21), written as

$$\tau_{\text{M}} \xrightarrow[\tau_{\text{S}} \gg 1]{} \frac{(1 + A_{\text{SP}}^2)\tau_{\text{S}}}{A_{\text{SP}}^2 \kappa_d \sqrt{\Omega_\mu}} \times 10^{\frac{f_{\text{sat}}^{\mu}}{10}}, \tag{32}$$

giving ToV [dB] $\rightarrow 10 \log_{10} \frac{(1+A_{\text{SP}}^2)\tau_{\text{S}}}{A_{\text{SP}}^2 \kappa_d \sqrt{\Omega_\mu}} + f_{\text{sat}}^{\mu}$. Note that this asymptote applies to $\mu = \texttt{RL}$ and $\texttt{RC}$, while the $\mu = \texttt{AWGN}$ case directly agrees with a simple formula (28).

3) RC Channel (Result 4-3): When $\mu = \texttt{RC}$, τ_{M} is determined by (33), as shown at the bottom of the next page, where it finds

$$\hat{\zeta} = \zeta \times 10^{\frac{f_{\text{co}}^{\text{RC|CE}}(\zeta_{\text{dB}}|\Theta_{\text{XPD}})}{10}}. \tag{34}$$

TABLE IX

COEFFICIENTS OF $f_{\mathrm{co}}^{\mathrm{RC|CE}}(\zeta_{\mathrm{dB}} \mid \Theta_{\mathrm{XPD}})$ W.R.T. XPD LEVELS

XPD Configuration Θ_{XPD}		Coefficients					
χ_L^{dB}	χ_N^{dB}	c_5	c_4	c_3	c_2	c_1	c_0
20 dB	20 dB	0	0	0	-5.331×10^{-6}	3.715×10^{-4}	0.416
	10 dB	0	0	-1.296×10^{-6}	8.327×10^{-5}	-1.628×10^{-3}	0.3982
	5 dB	0	0	-3.408×10^{-6}	2.372×10^{-4}	-5.249×10^{-3}	0.3658
	0 dB	3.05×10^{-8}	-2.178×10^{-6}	4.31×10^{-5}	1.382×10^{-4}	-1.185×10^{-2}	0.3149
10 dB	10 dB	0	7.126×10^{-8}	-2.277×10^{-6}	-1.175×10^{-4}	5.261×10^{-3}	0.4544
	5 dB	0	0	0	-1.566×10^{-5}	1.07×10^{-3}	0.4214
	0 dB	2.311×10^{-8}	-1.652×10^{-6}	3.44×10^{-5}	5.056×10^{-6}	-6.783×10^{-3}	0.367

TABLE X

VALUES OF $f_{\mathrm{sat}}^{\mathrm{RC}}$ AND THRESHOLDS OF SATURATION W.R.T. XPD LEVELS

XPD Configuration Θ_{XPD}		$f_{\mathrm{sat}}^{\mathrm{RC}}$ [dB]	$\mathrm{Th}(\Theta_{\mathrm{XPD}})$ [dB]
χ_L^{dB}	χ_N^{dB}		
20 dB	20 dB	0.42	25
	10 dB	0.39	20
	5 dB	0.33	20
	0 dB	0.22	20
10 dB	10 dB	0.50	20
	5 dB	0.44	30
	0 dB	0.31	20

for ζ following (12). The correction offset function in (34) is defined as

$$f_{\mathrm{co}}^{\mathrm{RC|CE}}(\zeta_{\mathrm{dB}}|\Theta_{\mathrm{XPD}}) = \begin{cases} \sum_{k=0}^{5} c_k \times (\zeta_{\mathrm{dB}})^k & \zeta_{\mathrm{dB}} < \mathrm{Th}(\Theta_{\mathrm{XPD}}) \\ f_{\mathrm{sat}}^{\mathrm{RC}} & \zeta_{\mathrm{dB}} \geq \mathrm{Th}(\Theta_{\mathrm{XPD}}), \end{cases} \tag{35}$$

where the coefficients $c_{k\in\{0,1,\cdots,5\}}$ and the saturation thresholds $\mathrm{Th}(\Theta_{\mathrm{XPD}})$ are provided in Tables IX and X, respectively, for each XPD configuration $(\chi_L^{\mathrm{dB}}, \chi_N^{\mathrm{dB}})$.

The asymptotic estimate for this RC channel case again coincides with (32). In fact, the validity condition may become rather stricter, requiring $\frac{(1+A_{\mathrm{SP}}^2)\tau_{\mathrm{S}}}{\sqrt{\Omega_\mu}} \gg 1 + K$.

B. Estimations in Layered MIMO Type A, CL

In this subsection, the CL-target mode of Class E procedure is addressed in the context of layered MIMO transmission. The proposed methods are summarized in *Result 5* and Algorithm 5 below.

§ *Result 5 (Class E estimates for LDM CL):* The Class E *ToV estimation* in CL-target mode is derived for each μ option, and is presented as the following *Results 5-1*, *5-2*, and *5-3*, corresponding to AWGN, RL, and RC cases. As in Section III-B.1, the ToV estimate for this mode is specially denoted by $\tau_{\mathrm{M}}^{\mathrm{CL}}$ throughout this section.

1) AWGN Channel (Result 5-1): Given μ = AWGN, Class E procedure yields

$$\tau_{\mathrm{M}}^{\mathrm{CL}} = \frac{\zeta_c}{\kappa_d}, \tag{36}$$

where ζ_c follows (26).

2) RL Channel (Result 5-2): For μ = RL, Class E estimate is given by

$$\tau_{\mathrm{M}}^{\mathrm{CL}} = \frac{(1+A_{\mathrm{SP}}^2)\zeta_r + \sqrt{\left(1+A_{\mathrm{SP}}^2\right)^2\zeta_r^2 + 4A_{\mathrm{SP}}^2\zeta_r}}{2A_{\mathrm{SP}}^2\kappa_d}, \tag{37}$$

where

$$\zeta_r = \frac{\hat{\zeta}_{\mathrm{CL}}}{1 - \Delta_{\mathrm{LDM}} - \Delta_{\mathrm{LDM}}\hat{\zeta}_{\mathrm{CL}}} \tag{38}$$

traces back to

$$\hat{\zeta}_{\mathrm{CL}} = \zeta_{\mathrm{CL}} \times 10^{\frac{f_{\mathrm{co}}^{\mu|\mathrm{CE}}(\zeta_{\mathrm{CL}}^{\mathrm{dB}}|\Theta_{\mathrm{XPD}})}{10}}. \tag{39}$$

Here, the parameters ζ_{CL} and $f_{\mathrm{co}}^{\mathrm{RL|CE}}(\cdot)$ revisited in (39) follow the definitions in Sections III-B and IV-A. That is, ζ_{CL} is given by (25); the same $f_{\mathrm{co}}^{\mathrm{RL|CE}}(\cdot)$ as in (31) is used while holding $\zeta_{\mathrm{CL}}^{\mathrm{dB}} = 10\log_{10}\zeta_{\mathrm{CL}}$ as input. The ζ_c appearing in (25) is given by (26).

3) RC Channel (Result 5-2): For μ = RC, $\tau_{\mathrm{M}}^{\mathrm{CL}}$ is given by (40) as shown at the bottom of the page,

where the ζ_r term follows (38) and (39) applies there, now with μ = RC. For (39) in this case, the same $f_{\mathrm{co}}^{\mathrm{RC|CE}}(\cdot)$ as in (35) is used while holding $\zeta_{\mathrm{CL}}^{\mathrm{dB}} = 10\log_{10}\zeta_{\mathrm{CL}}$ as input. Again, ζ_{CL} in (39) references (25), and the ζ_c appearing in (25) is given by (26).

C. Estimations in Layered MIMO Type A, EL

We now address the EL-target mode, with the proposed methods summarized in *Result 6* below. Throughout this

$$\tau_{\mathrm{M}} = \frac{(1+A_{\mathrm{SP}}^2)\hat{\zeta} - (1+K) + \sqrt{\left((1+A_{\mathrm{SP}}^2)\hat{\zeta} - (1+K)\right)^2 + 4A_{\mathrm{SP}}^2(1+K)\hat{\zeta}}}{2A_{\mathrm{SP}}^2\kappa_d} \tag{33}$$

$$\tau_{\mathrm{M}}^{\mathrm{CL}} = \frac{(1+A_{\mathrm{SP}}^2)\zeta_r - 1 - K + \sqrt{\left((1+A_{\mathrm{SP}}^2)\zeta_r - 1 - K\right)^2 + 4A_{\mathrm{SP}}^2(1+K)\zeta_r}}{2A_{\mathrm{SP}}^2\kappa_d} \tag{40}$$

Algorithm 5 Class E Procedure for CL (layered MIMO)

Input: τ_{S}, μ, Θ_{XPD}, F_{PB}, D_X, D_Y, and δ.

procedure CLASS E, LDM CL
  Initialization Compute $\mathcal{E}_R$, Ω_μ, A_{SP}, κ_d, and Δ_{LDM}.
  Step 1: Compute ζ_c using (26).
  Step 2:
  if $\mu = \texttt{AWGN}$ **then**
    Obtain $\tau_{\mathrm{M}}^{\mathrm{CL}}$ using (36).
    end procedure.
  else
    Obtain ζ_{CL} by (25).
    Proceed to **Step 3**.
  end if
  Step 3: Compute $\hat{\zeta}_{\mathrm{CL}} = \zeta_{\mathrm{CL}} \times 10^{\frac{f_{\mathrm{co}}^{\mu|\mathrm{CE}}(\zeta_{\mathrm{CL}}^{\mathrm{dB}}|\Theta_{\mathrm{XPD}})}{10}}$.
    ▹ Apply (31) if $\mu = \texttt{RL}$, and (35) if $\mu = \texttt{RC}$.
      ▹ Use $\zeta_{\mathrm{CL}}^{\mathrm{dB}} = 10\log_{10}\zeta_{\mathrm{CL}}$.
  Step 4: Convert $\hat{\zeta}_{\mathrm{CL}}$ into ζ_r using (38).
  Step 5: Obtain $\tau_{\mathrm{M}}^{\mathrm{CL}}$ from (37).
end procedure
return $\tau_{\mathrm{M}}^{\mathrm{CL}}$.

Algorithm 6 Class E Procedure for EL (layered MIMO)

Input: τ_{S}, μ, Θ_{XPD}, F_{PB}, D_X, D_Y, and δ.

procedure CLASS E, LDM EL
  Initialization Compute $\mathcal{E}_R$, Ω_μ, A_{SP}, κ_d, and Δ_{LDM}.
  Step 1: Compute ζ using (12).
  Step 2: Convert ζ into ζ_{EL} using (45).
    ▹**if**$\mu = \texttt{AWGN}$ **then**
    ▹ Apply $f_{\mathrm{co}}^{\mathrm{AWGN|CE}}(\zeta_{\mathrm{dB}}|\Theta_{\mathrm{XPD}}) = 0$.
    ▹ **else**
    ▹ Apply (31) if $\mu = \texttt{RL}$, and (35) if $\mu = \texttt{RC}$.
    ▹ **end if**
  Step 3: Obtain $\tau_{\mathrm{M}}^{\mathrm{EL}}$ from (41).
      Use (42)-(44), depending on μ.
end procedure
return $\tau_{\mathrm{M}}^{\mathrm{EL}}$.

section, the ToV estimate for this mode is denoted by $\tau_{\mathrm{M}}^{\mathrm{EL}}$, consistent with Section III-B.2.

§ *Result 6 (Class E estimates for LDM EL):* The estimate $\tau_{\mathrm{M}}^{\mathrm{EL}}$ is determined as

$$\tau_{\mathrm{M}}^{\mathrm{EL}} = \begin{cases} \tau_{\mathrm{M}}^{\mathrm{EL}}|_{\texttt{AWGN}} & \mu = \texttt{AWGN} \\ \tau_{\mathrm{M}}^{\mathrm{EL}}|_{\texttt{RL}} & \mu = \texttt{RL} \\ \tau_{\mathrm{M}}^{\mathrm{EL}}|_{\texttt{RC}} & \mu = \texttt{RC}, \end{cases} \tag{41}$$

with (42)–(44), as shown at the bottom of the next page, specifying the respective realizations.

Each case traces back to the intermediate estimate

$$\zeta_{\mathrm{EL}} = \frac{\zeta}{\Delta_{\mathrm{LDM}}} \times 10^{\frac{f_{\mathrm{co}}^{\mu|\mathrm{CE}}(\zeta_{\mathrm{dB}}|\Theta_{\mathrm{XPD}})}{10}}, \tag{45}$$

which finds ζ and Δ_{LDM} at (12) and (24). The correction function $f_{\mathrm{co}}^{\mu|\mathrm{CE}}(\cdot)$ is the same as described in Section IV-A for each μ. For $\mu = \texttt{AWGN}$, $f_{\mathrm{co}}^{\mathrm{AWGN|CE}}(\cdot)$ is set to zero.

The procedure in this mode unfolds as Algorithm 6. Overall, the estimation procedure for LDM EL closely parallels that of the SL case in Section III-B.2, with the main distinction being the scaling of ζ by $1/\Delta_{\mathrm{LDM}}$ in the process.

V. DERIVATIONS AND PROOFS PART I: CLASS P

This section traces back to detailed derivations underlying Class P results. Sections V-A, -B, and -C tackle *Result 1*, *Result 2*, and *Result 3* in order.

A. Derivation of Result 1: Class P, SL

Every result is drawn from channel capacity matching. That is, we determine τ_{M} by matching the MIMO mutual information (MI) to twice the SISO capacity at τ_{S}. According to the signal model in (1), the instantaneous MI for SL MIMO amounts to

$$I_{\mathrm{MI}}(\Gamma) = \log\det\bigl(\mathbf{I} + \Gamma\mathbf{H}\mathbf{H}^H\bigr) \tag{46}$$

with optimal ML MIMO equalization [8], where $\Gamma = \frac{P_R}{\sigma_n^2}$ denotes the received CNR per polarization. The ergodic MI averaged over $\mathbf{H}$ ensembles, $\mathbb{E}_{\mathbf{H}}[I_{\mathrm{MI}}(\Gamma)]$, then yields an inequality

$$\mathbb{E}_{\mathbf{H}}[I_{\mathrm{MI}}(\Gamma)] \le \log\mathbb{E}_{\mathbf{H}}\bigl[\det\bigl(\mathbf{I} + \Gamma\mathbf{H}\mathbf{H}^H\bigr)\bigr] \triangleq \tilde{I}_{\mathrm{MI}}(\Gamma) \tag{47}$$

that relies on Jensen's inequality over a concave log function. We first approximate the ergodic MI by $\tilde{I}_{\mathrm{MI}}(\Gamma)$ to obtain ζ and apply correction offsets afterhand.

On the other hand, the SISO capacity at τ_{S} is directly given by $C_{\mathrm{SISO}} = \log(1+\tau_{\mathrm{S}})$. We then solve MI matching for Γ such that

$$\mathbb{E}_{\mathbf{H}}[I_{\mathrm{MI}}(\Gamma)] = 2C_{\mathrm{SISO}} \tag{48}$$

and define the solution as the Class P estimate τ_{M}.

1) AWGN Channel: With $\mathbf{H} = \mathbf{H}_{\mathrm{AWGN}}$ given by Table I, a simple algebra on (46) gives

$$\begin{aligned} e^{\mathbb{E}_{\mathbf{H}}[I_{\mathrm{MI}}(\Gamma)]} &= 1 + \Gamma\sum_{i,j}|h_{ij}|^2 + \Gamma^2|h_{00}h_{11} - h_{01}^*h_{10}^*|^2 \\ &= 1 + 2\Gamma + \Omega_{\mathrm{AWGN}}\Gamma^2. \end{aligned} \tag{49}$$

Note here that $\mathbf{H}_{\mathrm{AWGN}}$ is pure-deterministic so $I_{\mathrm{MI}}(\Gamma) = \mathbb{E}_{\mathbf{H}}[I_{\mathrm{MI}}(\Gamma)] = \tilde{I}_{\mathrm{MI}}(\Gamma)$ directly holds, and the expectation in (49) is hence neglected.

The previous definition (13) is an abbreviation of $e^{2C_{\mathrm{SISO}}} = (1+\tau_{\mathrm{S}})^2 \triangleq \mathcal{E}_R$. The objective is then solving a quadratic equation $\Omega_{\mathrm{AWGN}}\tau_{\mathrm{M}}^2 + 2\tau_{\mathrm{M}} + 1 - \mathcal{E}_R = 0$, which straightforwardly yields (16), equivlalently, (10) and (12) with $f_{\mathrm{co}}^{\mathrm{AWGN}}(\zeta_{\mathrm{dB}}|\Theta_{\mathrm{XPD}}) = 0$. □

2) RL Channel: On the other hand, $\mathbf{H} = \mathbf{H}_{\mathrm{RL}}$ gives

$$\begin{aligned} &e^{\tilde{I}_{\mathrm{MI}}(\Gamma)} \\ &= 1 + \Gamma\mathbb{E}_{\mathbf{H}_{\mathrm{RL}}}\left[\sum_{i,j}|h_{ij}|^2\right] + \Gamma^2\mathbb{E}_{\mathbf{H}_{\mathrm{RL}}}\bigl[|h_{00}h_{11} - h_{01}^*h_{10}^*|^2\bigr] \\ &= 1 + 2\Gamma + \Omega_{\mathrm{RL}}\Gamma^2 \end{aligned} \tag{50}$$

that includes expectations over ensembles of $\mathbf{H}_{\mathrm{RL}}$. ζ in (12) is then obtained accordingly from $\Omega_{\mathrm{RL}}\zeta^2 + 2\zeta + 1 - \mathcal{E}_R = 0$, a spell-out of (48).

Note from (47) that a gap exists between $\mathbb{E}_{\mathbf{H}}[I_{\mathrm{MI}}(\Gamma)]$ and $\tilde{I}_{\mathrm{MI}}(\Gamma)$ in general. Prior work has highlighted the analytical

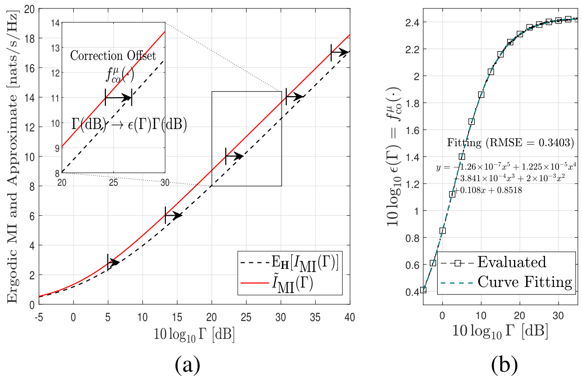

Fig. 1. Illustration of $f^{\mu}_{\mathrm{co}}(\zeta_{\mathrm{dB}}|\Theta_{\mathrm{XPD}})$ ($\mu = \mathtt{RL}$, $\chi^{\mathrm{dB}}_{N} = 10$ [dB]).

intractability of ergodic MI and developed deterministic equivalents, e.g., [52], [53]. However, these results are typically asymptotic, valid only in the large-scale MIMO limit, and too complex for our model.

Thus, a two-step process is adopted: (*i*) Solve $\tilde{I}_{\mathrm{MI}}(\zeta) = 2C_{\mathrm{SISO}}$ for a tractable proxy ζ; and (*ii*) apply a correction offset to bring ζ to τ_{M}, which satisfies $\mathbb{E}_{\mathbf{H}}[I_{\mathrm{MI}}(\tau_{\mathrm{M}})] = 2C_{\mathrm{SISO}}$. From (47), it can be deduced that achieving $\tilde{I}_{\mathrm{MI}}(\Gamma)$ with $\mathbb{E}_{\mathbf{H}}[I_{\mathrm{MI}}(\Gamma')]$ requires a larger CNR $\Gamma' \geq \Gamma$. Accordingly, one can find, for each Γ, a scaling factor $\epsilon(\Gamma) \geq 1$ such that

$$\mathbb{E}_{\mathbf{H}}[I_{\mathrm{MI}}(\epsilon(\Gamma)\Gamma)] = \tilde{I}_{\mathrm{MI}}(\Gamma). \tag{51}$$

With $\epsilon(\Gamma)$ known, final estimate can proceed with $\tau_{\mathrm{M}} = \epsilon(\zeta)\zeta$. To this end, we numerically established parametric fits for $\epsilon(\Gamma)$. The correction offset function $f^{\mu}_{\mathrm{co}}(\zeta_{\mathrm{dB}}|\Theta_{\mathrm{XPD}}) = 10\log_{10}\epsilon(\zeta)|_{\Theta_{\mathrm{XPD}}}$ is the specific realization of $\epsilon(\zeta)$. Note that a dB-domain representation is adopted to align with industry practice. For selected XPD configurations (see Table II) and a dense set of Γs including $[-5, 40]$ dB range, $\mathbb{E}_{\mathbf{H}}[I_{\mathrm{MI}}(\Gamma)]$s were computed over Monte Carlo ensembles of $\mathbf{H}_{\mathrm{RL}}$. The gap to the closed-form $\tilde{I}_{\mathrm{MI}}(\Gamma)$ was quantified thereon; and curve fitting consequently produced (18) with coefficients in Tables IV and V. See Fig. 1 for an example illustration. The values of f^{μ}_{sat} were derived in integral form involving Bessel functions, which still required numerical computation to evaluate.

Collecting the results (10), (12), (18), Tables IV and V completes the derivation. □

3) RC Channel: This case is also addressed similarly. (12) is extracted from $\Omega_{\mathrm{RC}}\zeta^2 + 2\zeta + 1 - \mathcal{E}_R = 0$, where Ω_{RC} refers to (19). A numerical process fabricated the correction offset function $f^{\mathrm{RC}}_{\mathrm{co}}(\zeta_{\mathrm{dB}}|\Theta_{\mathrm{XPD}})$ in the same fashion. □

B. Derivation of Result 2: Class P, Layered MIMO CL

When $\mathcal{I}(a;b)$ dictates the MI between random variables a and b, the achievable rate of CL amounts to

$$\begin{aligned} I^{\mathrm{CL}}_{\mathrm{MI}}(\Gamma) &= \mathcal{I}(\mathbf{x}_c;\mathbf{y}|\mathbf{H}) \\ &= \log\det\bigl(\mathbf{I} + \Gamma\mathbf{H}\mathbf{H}^H\bigr) - \log\det\bigl(\mathbf{I} + \Delta_{\mathrm{LDM}}\Gamma\mathbf{H}\mathbf{H}^H\bigr) \end{aligned} \tag{52}$$

for an instantaneous $\mathbf{H}$. For later notational convenience, let us define

$$\mathcal{I}_o(\gamma, \mathbf{A}) \triangleq \log\det\bigl(\mathbf{I} + \gamma\mathbf{A}\mathbf{A}^H\bigr) \tag{53}$$

for $^{\forall}\gamma \in \mathbb{R}^+$ and $^{\forall}\mathbf{A} \in \mathbb{C}^{2\times 2}$. Then, (52) above can be concisely rewritten by $I^{\mathrm{CL}}_{\mathrm{MI}}(\Gamma) = \mathcal{I}_o(\Gamma, \mathbf{H}) - \mathcal{I}_o(\Delta_{\mathrm{LDM}}\Gamma, \mathbf{H})$. In subsequence proceeding with ergodic metrics, applying Jensen approximation to each I_o term in $\mathbb{E}_{\mathbf{H}}[I^{\mathrm{CL}}_{\mathrm{MI}}(\Gamma)]$ yields a Jensen-type approximation

$$\mathbb{E}_{\mathbf{H}}[I^{\mathrm{CL}}_{\mathrm{MI}}(\Gamma)] \approx \tilde{I}^{\mathrm{CL}}_{\mathrm{MI}}(\Gamma) \triangleq \log\left(\frac{1 + 2\Gamma + \Omega_{\mu}\Gamma^2}{1 + 2\Delta_{\mathrm{LDM}}\Gamma + \Omega_{\mu}\Delta^2_{\mathrm{LDM}}\Gamma^2}\right). \tag{54}$$

1) AWGN Channel: Given $\mathbf{H} = \mathbf{H}_{\mathrm{AWGN}}$, $\mathbb{E}_{\mathbf{H}}[I_{\mathrm{MI}}(\gamma_{\mathrm{CL}})] = \tilde{I}^{\mathrm{CL}}_{\mathrm{MI}}(\Gamma)$ holds directly since randomness in $\mathbf{H}$ is precluded. The matching $\mathbb{E}_{\mathbf{H}}[I_{\mathrm{MI}}(\tau_{\mathrm{M}})] = 2C_{\mathrm{SISO}}$ promptly turns out to form a quadratic equation $\Omega_{\mathrm{AWGN}}(1-\mathcal{E}_R\Delta^2_{\mathrm{LDM}})\tau^2_{\mathrm{M}} + 2(1-\mathcal{E}_R\Delta_{\mathrm{LDM}})\tau_{\mathrm{M}} + 1 - \mathcal{E}_R = 0$, which results in $\tau_{\mathrm{M}} = \zeta_c$ where ζ_c complies with (26) with $\mu = \mathtt{AWGN}$. □

2) RL Channel: The difference-of-log form of $I^{\mathrm{CL}}_{\mathrm{MI}}(\Gamma)$ complicates a direct CNR correction from $\tilde{I}^{\mathrm{CL}}_{\mathrm{MI}}(\Gamma)$ toward $\mathbb{E}_{\mathbf{H}}[I^{\mathrm{CL}}_{\mathrm{MI}}(\epsilon(\Gamma)\Gamma)]$. Alternatively, we can make a detour assisted by a Padé approximation

$$\begin{aligned} I^{\mathrm{CL}}_{\mathrm{MI}}(\Gamma) &= \sum_{i=1,2}\log\det\left(\mathbf{I} + \frac{(1-\Delta_{\mathrm{LDM}})\Gamma\lambda_i}{1+\Delta_{\mathrm{LDM}}\Gamma\lambda_i}\right) \\ &\approx \log\det\bigl(\mathbf{I} + \Phi(\Gamma)\mathbf{H}\mathbf{H}^H\bigr) = \mathcal{I}_o(\Phi(\Gamma), \mathbf{H}), \end{aligned} \tag{55}$$

where λ_1 and λ_2 denote the 1st and 2nd eigenvalues of $\mathbf{H}\mathbf{H}^H$, respectively; and

$$\Phi(\Gamma) \triangleq \frac{(1-\Delta_{\mathrm{LDM}})\Gamma}{1+\Delta_{\mathrm{LDM}}\Gamma} \tag{56}$$

defines a Möbius transformation to an auxiliary equivalent. This approximation in (55) appears tight for small $\Delta_{\mathrm{LDM}}\Gamma$, where ATSC 3.0's recommended setting $\delta\tau_{\mathrm{M}} < \frac{1}{2}$ supports this regime.[11] The tightness is numerically examined later in Section VIII. Intuitively, (55) can be interpreted as a model

[11] A/327 states: Given a ModCod setting $\mathcal{S}$ for the CL, and letting τ_{SL} denote the ToV for SL transmission under $\mathcal{S}$, select a δ such that $\delta\tau_{\mathrm{SL}} < \frac{1}{2}$ for valid LDM operation, ensuring a 3 dB margin [54].

$$\tau^{\mathrm{EL}}_{\mathrm{M}}|_{\mathtt{AWGN}} = \frac{\zeta_{\mathrm{EL}}}{\kappa_d} \tag{42}$$

$$\tau^{\mathrm{EL}}_{\mathrm{M}}|_{\mathtt{RL}} = \frac{(1+A^2_{\mathrm{SP}})\zeta_{\mathrm{EL}} + \sqrt{\left(1+A^2_{\mathrm{SP}}\right)^2\zeta^2_{\mathrm{EL}} + 4A^2_{\mathrm{SP}}\zeta_{\mathrm{EL}}}}{2A^2_{\mathrm{SP}}\kappa_d} \tag{43}$$

$$\tau^{\mathrm{EL}}_{\mathrm{M}}|_{\mathtt{RC}} = \frac{(1+A^2_{\mathrm{SP}})\zeta_{\mathrm{EL}} - 1 - K + \sqrt{((1+A^2_{\mathrm{SP}})\zeta_{\mathrm{EL}} - 1 - K)^2 + 4A^2_{\mathrm{SP}}(1+K)\zeta_{\mathrm{EL}}}}{2A^2_{\mathrm{SP}}\kappa_d} \tag{44}$$

treating the interference-like terms as additive white noise, reducing the system into an equivalent SL case with the desired signal's strength $(1-\Delta_{\mathrm{LDM}})P_R$ and effective noise power $\sigma_n^2 + \Delta_{\mathrm{LDM}} P_R$ on each polarization.

The first surrogate ζ_c is defined as the solution to $\tilde{I}_{\mathrm{MI}}^{\mathrm{CL}}(\zeta_c) = 2C_{\mathrm{SISO}}$ using (54). Rearranging reduces this condition to a quadratic in ζ_c and results in (26).

The remaining proceeds with connecting ζ_c and $\tilde{I}_{\mathrm{MI}}^{\mathrm{CL}}(\zeta_c)$ to $\mathbb{E}_{\mathbf{H}}[I_{\mathrm{MI}}^{\mathrm{CL}}(\tau_{\mathrm{M}})]$ via $\mathbb{E}_{\mathbf{H}}[\mathcal{I}_o(\Phi(\zeta_c), \mathbf{H})]$. Note that ζ_{CL} in (25) can be written as $\zeta_{\mathrm{CL}} = \Phi(\zeta_c)$. To this end, we define an invertible mapping

$$\mathcal{M} : \tilde{I}_{\mathrm{MI}}^{\mathrm{CL}} \mapsto \tilde{J} \quad \text{s.t.} \quad \tilde{I}_{\mathrm{MI}}^{\mathrm{CL}}(\Gamma) = \tilde{J}(\Phi(\Gamma)). \tag{57}$$

The same mapping $\mathcal{M}$ also defines $J_E(\cdot)$ by

$$\mathcal{M} : \mathbb{E}_{\mathbf{H}}[I_{\mathrm{MI}}^{\mathrm{CL}}] \mapsto J_E \quad \text{s.t.} \quad \mathbb{E}_{\mathbf{H}}[I_{\mathrm{MI}}^{\mathrm{CL}}(\Gamma)] = J_E(\Phi(\Gamma)). \tag{58}$$

Additionally, responding to the definition of a scenario-independent function $\mathcal{I}_o(\gamma, \mathbf{A})$, let the Jensen approximation of $\mathbb{E}_{\mathbf{A}}[\mathcal{I}_o(\gamma, \mathbf{A})]$ defined as

$$\tilde{\mathcal{I}}_o(\gamma, \mathcal{A}) \triangleq \log \mathbb{E}_{\mathbf{A}\in\mathcal{A}}\left[\det\left(\mathbf{I} + \gamma \mathbf{A}\mathbf{A}^H\right)\right] \tag{59}$$

for $\mathcal{A}$ denoting the ensemble set of $\mathbf{A}$. Note that in a domain of $\gamma_{\mathrm{CL}} \triangleq \Phi(\Gamma)$, we already have a heuristic mapping $\epsilon(\cdot)$ discussed in Section V-A that gives $\tilde{\mathcal{I}}_o(\gamma_{\mathrm{CL}}, \mathcal{H}) = J_E(\epsilon(\gamma_{\mathrm{CL}})\gamma_{\mathrm{CL}})$ when we denote the ensemble set of $\mathbf{H}$ by $\mathcal{H}$. Stepwise, approximating $\tilde{J}(\zeta_{\mathrm{CL}}) \approx \tilde{\mathcal{I}}_o(\gamma_{\mathrm{CL}}, \mathcal{H})$ on the ζ_{CL}-domain therefore leads to $\hat{\zeta}_{\mathrm{CL}}$ in (23). Subsequently, an inverse mapping $\mathcal{M}^{-1} : J_E \mapsto \mathbb{E}_{\mathbf{H}}[I_{\mathrm{MI}}^{\mathrm{CL}}]$, equivalently with $\Phi^{-1}(\gamma_{\mathrm{CL}}) = \frac{\gamma_{\mathrm{CL}}}{1-\Delta_{\mathrm{LDM}}-\Delta_{\mathrm{LDM}}\gamma_{\mathrm{CL}}}$, we get $\tau_{\mathrm{M}} = \Phi^{-1}(\hat{\zeta}_{\mathrm{CL}})$ in (22).

§ *Remark: Further improvement*

More tighter results may be obtained by using $\Phi(\Gamma) = \frac{(1-\Delta_{\mathrm{LDM}})\Gamma}{1+2\Delta_{\mathrm{LDM}}\Gamma}$ instead of $\frac{(1-\Delta_{\mathrm{LDM}})\Gamma}{1+\Delta_{\mathrm{LDM}}\Gamma}$. In that case, (22) will alternatively be $\tau_{\mathrm{M}}^{\mathrm{CL}} = \Phi^{-1}(\hat{\zeta}_{\mathrm{CL}}) = \frac{\hat{\zeta}_{\mathrm{CL}}}{1-\Delta_{\mathrm{LDM}}-2\Delta_{\mathrm{LDM}}\hat{\zeta}_{\mathrm{CL}}}$ and (25) will be $\zeta_{\mathrm{CL}} = \Phi(\zeta_c) = \frac{(1-\Delta_{\mathrm{LDM}})\zeta_c}{1+2\Delta_{\mathrm{LDM}}\zeta_c}$. □

3) RC Channel: The RC channel case can be tackled in a similar manner to the RL case described above. □

C. Derivation of Result 3: Class P, Layered MIMO EL

Note in (3) that the EL signal model is a scaled version of SL's. It is assumed that SIC is perfectly accomplished, ensuring interference-free reception by removing all CL components. The only difference is a power reduced by Δ_{LDM}. Simple shifts by Δ_{LDM} yield the presented results. □

VI. Derivations and Proofs Part II: Class E

The ideas in Section V extend to scenarios with imperfect CSIR. Unlike the perfect CSIR case, the exact capacity is generally unknown in this regime; instead, the generalized MI (GMI) of Lapidoth and Shamai [55] provides an accessible measure, which establishes a computable MI lower bound [56], [57]

$$\begin{aligned}\mathcal{I}(\mathbf{x}; \mathbf{y}|\hat{\mathbf{H}}) &\geq \log\det\left(\mathbf{I} + \Gamma_d \hat{\mathbf{H}}^H (\mathbf{I} + \Gamma_d \boldsymbol{\Sigma})^{-1} \hat{\mathbf{H}}\right) \\ &\triangleq I_{\mathrm{GMI}}(\Gamma), \end{aligned} \tag{60}$$

where $\Gamma_d \triangleq \kappa_d \Gamma$, $\boldsymbol{\Sigma} \triangleq \mathbb{E}_{\tilde{\mathbf{H}}}[\tilde{\mathbf{H}}\mathbf{x}\mathbf{x}^H\tilde{\mathbf{H}}^H] = \Gamma_d \mathbb{E}_{\tilde{\mathbf{H}}}[\tilde{\mathbf{H}}\tilde{\mathbf{H}}^H]$. We employ this GMI as an alternative to the exact MI.

As discussed in Section II-A.2, pilot boosting may redistribute power between data and pilot signals, thereby mediating the tradeoff between data signal quality and channel estimation accuracy. Accordingly, we specially denote the data signal CNR by $\Gamma_d = \frac{P_d}{\sigma_n^2} = \kappa_d \Gamma$, and the pilot signal's average CNR by $\Gamma_p = \frac{P_p}{2\sigma_n^2} = A_{\mathrm{SP}}^2 \kappa_d \Gamma$. The definition of κ_d follows (8).

$\hat{\mathbf{H}}$ and $\tilde{\mathbf{H}}$ are characterized by LMMSE channel estimation over pilot observations, where the pilot topology conforms to (7) described in Section II-A.2. Shortly, a pilot observation $\mathbf{Y}_p = \mathbf{HP} + \mathbf{N}$ yields the estimate

$$\hat{\mathbf{H}} = \mathbf{Y}_p(\mathbf{P}^H \mathbf{R}_{\mathbf{H}} \mathbf{P} + 2\sigma_n^2 \mathbf{I})^{-1} \mathbf{P} \mathbf{R}_{\mathbf{H}} \tag{61}$$

where $\mathbf{N} \in \mathbb{C}^{2\times 2}$ is a thermal noise matrix whose entries all follow i.i.d. $\mathcal{CN}(0, \sigma_n^2)$; $\mathbf{R}_{\mathbf{H}} = \mathbb{E}_{\mathbf{H}}[\mathbf{H}\mathbf{H}^H]$ denotes the covariance matrix of $\mathbf{H}$. Statistical properties of $\hat{\mathbf{H}}$ and $\tilde{\mathbf{H}}$ will be detailed in the following subsections as specific to each channel model.

As with Section V, we set an approximate proxy $\tilde{I}_{\mathrm{GMI}}(\Gamma) = \log \mathbb{E}_{\hat{\mathbf{H}}}[\det(\mathbf{I} + \Gamma_d \boldsymbol{\Sigma} + \Gamma_d \hat{\mathbf{H}}\hat{\mathbf{H}}^H)] - \log\det(\mathbf{I} + \Gamma_d \boldsymbol{\Sigma})$ to draw intermediate surrogates. This approximation $\tilde{I}_{\mathrm{GMI}}(\Gamma)$ satisfies a Jensen's inequality $\mathbb{E}_{\hat{\mathbf{H}}}[I_{\mathrm{GMI}}(\Gamma)] \leq \tilde{I}_{\mathrm{GMI}}(\Gamma)$.

A. Derivation of Result 4: Class E, SL

1) Derivation of Result 4-1 (AWGN): With long-term observation that averages the channel gain bias, the MMSE estimator provides an exact channel estimate in the AWGN case. The only remaining effect is the reduction of data power due to pilot boosting. Hence, the problem is reduced to that of Section III-A.1 (Class P, SL) with power scaling by κ_d, yielding $\tau_{\mathrm{M}} = \frac{\zeta}{\kappa_d}$ for ζ given in (12) with $\mu = \mathtt{AWGN}$. □

2) Derivation of Result 4-2 (RL): Let $\hat{h}_{ij}$ denote the estimate of h_{ij}, and define the error as $\tilde{h}_{ij} = h_{ij} - \hat{h}_{ij}$, for $i, j \in \{0, 1\}$. Given $\mathbf{H} = \mathbf{H}_{\mathrm{RL}}$ and based on (61), the diagonal entries of $\hat{\mathbf{H}}$ and $\tilde{\mathbf{H}}$ turn out to follow $\hat{h}_{00}, \hat{h}_{11} \sim \mathcal{CN}\left(0, \frac{\Gamma_p + 2\rho_N \Gamma_p^2}{2(1+\Gamma_p)^2}\right)$ and $\tilde{h}_{00}, \tilde{h}_{11} \sim \mathcal{CN}\left(0, \frac{2\rho_N + \Gamma_p}{2(1+\Gamma_p)^2}\right)$, while the off-diagonal entries follow $\hat{h}_{10}, \hat{h}_{01} \sim \mathcal{CN}\left(0, \frac{\Gamma_p + 2(1-\rho_N)\Gamma_p^2}{2(1+\Gamma_p)^2}\right)$ and $\tilde{h}_{10}, \tilde{h}_{01} \sim \mathcal{CN}\left(0, \frac{2(1-\rho_N) + \Gamma_p}{2(1+\Gamma_p)^2}\right)$. Conservatively, $\mathbf{R}_{\mathbf{H}} = \mathbf{I}$ is used, corresponding to typical receivers that do not possess prior knowledge of channel XPD.[12]

The specified properties of $\hat{\mathbf{H}}$ and $\tilde{\mathbf{H}}$ imply the corollary $\boldsymbol{\Sigma} = \mathbb{E}_{\mathbf{H}}[\tilde{\mathbf{H}}\tilde{\mathbf{H}}^H] = \frac{1}{1+\Gamma_p}\mathbf{I}$, which in turn realizes

$$\begin{aligned} I_{\mathrm{GMI}}(\Gamma) &= \log\det\left(\mathbf{I} + \Gamma_d \boldsymbol{\Sigma} + \Gamma_d \hat{\mathbf{H}}\hat{\mathbf{H}}^H\right) - \log\det(\mathbf{I} + \Gamma_d \boldsymbol{\Sigma}) \\ &= \log\det\left(\mathbf{I} + \frac{\Gamma_d}{1 + \frac{\Gamma_d}{1+\Gamma_p}} \hat{\mathbf{H}}\hat{\mathbf{H}}^H\right). \end{aligned}$$

The Jensen approximation of $\mathbb{E}_{\hat{\mathbf{H}}}[I_{\mathrm{GMI}}(\Gamma)]$, denoted $\tilde{I}_{\mathrm{GMI}}(\Gamma)$, is then given by (62), as shown at the bottom of the next page. Here, we use asymptotic approximations obtained in the

[12] With receivers having prior knowledge of XPD, the channel estimates can be improved with $\{\mathrm{Var}(\hat{h}_{ij}), \mathrm{Var}(\tilde{h}_{ij})\} = \left\{\frac{\Gamma_p u_\rho^2}{1+\Gamma_p u_\rho}, \frac{u_\rho}{1+\Gamma_p u_\rho}\right\}$, as in [7], where $u_\rho = \rho_N$ (diagonal) or $u_\rho = 1 - \rho_N$ (off-diagonal).

extreme regimes: In the high-CNR[13] regime $\Gamma \gg 1$, (62) can be recast as

$$e^{\tilde{I}_{\text{GMI}}(\Gamma)} \approx 1 + \frac{2\Gamma_d\Gamma_p}{1+\Gamma_d+\Gamma_p} + \frac{\Omega_{\text{RL}}\Gamma_d^2\Gamma_p^2}{(1+\Gamma_d+\Gamma_p)^2} \tag{63}$$

by applying $\frac{\Gamma_p}{1+\Gamma_p} \to 1$ and $\frac{2\Gamma_p+1}{2\Omega_{\text{RL}}\Gamma_p^2} \to 0$. The approximation of $\tilde{I}_{\text{GMI}}(\Gamma)$ implied by (63) is hereafter denoted by $\hat{I}_{\text{GMI}}(\Gamma)$ in this subsection.

Let us define

$$\nu_\mu(\gamma) \triangleq 1 + 2\gamma + \Omega_\mu\gamma^2, \quad {}^\forall\gamma \in \mathbb{R}^+, \tag{64}$$

and

$$\psi_{\text{RL}}(\Gamma) \triangleq \frac{\Gamma_d\Gamma_p}{1+\Gamma_d+\Gamma_p} = \frac{A_{\text{SP}}^2\kappa_d^2\Gamma^2}{1+(1+A_{\text{SP}}^2)\kappa_d\Gamma}, \tag{65}$$

for notational convenience. Then, $\hat{I}_{\text{GMI}}(\Gamma') = 2C_{\text{SISO}}$ determines $\nu_{\text{RL}}(\zeta) = \mathcal{E}_R$ for $\zeta = \psi_{\text{RL}}(\Gamma')$, from which the expression of ζ in (12) follows.

This result coincides with that derived in the low-CNR regime. For $\Gamma \ll 1$, $e^{\tilde{I}_{\text{GMI}}(\Gamma)} \approx 1 + 2\psi_{\text{RL}}(\Gamma)$ straightforwardly yields $\zeta = \frac{\mathcal{E}_R-1}{2}$ when ζ is defined as $\psi_{\text{RL}}(\Gamma)$ satisfying $\tilde{I}_{\text{GMI}}(\Gamma) = 2C_{\text{SISO}}$. The approximative form of (12) under $\Omega_\mu(\mathcal{E}_R-1) \ll 1$ also reduces to $\frac{\mathcal{E}_R-1}{2}$, using $\sqrt{1+x} \approx 1+\frac{x}{2}$, thereby confirming consistency.

Following the approach in Section V, the scaling factor is heuristically determined to correct the approximation gap. Note that the scaling factor $\epsilon(\cdot)$ is found on the domain $\zeta' = \psi_{\text{RL}}(\Gamma)$ such that $\hat{I}_{\text{GMI}}(\psi_{\text{RL}}^{-1}(\zeta')) = \mathbb{E}_{\hat{\mathbf{H}}}[I_{\text{GMI}}(\psi_{\text{RL}}^{-1}(\epsilon(\zeta')\zeta'))]$. As described in Section V-A.2, $\mathbb{E}_{\hat{\mathbf{H}}}[I_{\text{GMI}}]$ was evaluated using Monte Carlo ensembles of $\hat{\mathbf{H}}|_{\mu=\mathtt{RL}}$, and the gap relative to the closed-form $\hat{I}_{\text{GMI}}$ was quantified there. The realized form of $\epsilon(\cdot)$ in this scenario is $f_{\text{co}}^{\text{RL|CE}}(\zeta'_{\text{dB}}|\Theta_{\text{XPD}})$ in (31), where $\zeta'_{\text{dB}} = 10\log_{10}\zeta'$.

Thus, the corrected surrogate in (30) is $\hat{\zeta} = \epsilon(\zeta)\zeta$ that achieves $\mathbb{E}_{\hat{\mathbf{H}}}\left[I_{\text{GMI}}\left(\psi_{\text{RL}}^{-1}(\hat{\zeta})\right)\right] = 2C_{\text{SISO}}$. Returning to the original domain via $\tau_{\text{M}} = \psi_{\text{RL}}^{-1}(\hat{\zeta})$ yields the final estimate, as given in (29). The inverse operation of $\psi_{\text{RL}}(\cdot)$ can be readily derived from (65). □

3) Derivation of Result 4-3 (RC): Given $\mathbf{H} = \mathbf{H}_{\text{RC}}$ and based on (61), the diagonal and off-diagonal entries of $\hat{\mathbf{H}}$ follow $\mathcal{CN}\left(\sqrt{\frac{K\rho_L}{1+K}}, \frac{\Gamma_p+\frac{2\rho_N\Gamma_p^2}{1+K}}{2(1+K+\Gamma_p)^2}\right)$ and $\mathcal{CN}\left(\sqrt{\frac{K(1-\rho_L)}{1+K}}, \frac{\Gamma_p+\frac{2(1-\rho_N)\Gamma_p^2}{1+K}}{2(1+K+\Gamma_p)^2}\right)$, respectively. Similarly, the diagonal and off-diagonal entries of $\tilde{\mathbf{H}}$ follow $\mathcal{CN}\left(0, \frac{2(1+K)\rho_N+\Gamma_p}{2(1+K+\Gamma_p)^2}\right)$ and $\mathcal{CN}\left(0, \frac{2(1+K)(1-\rho_N)+\Gamma_p}{2(1+K+\Gamma_p)^2}\right)$, respectively. Note that the LoS components are accurately estimated, as discussed in Section VI-A.1. The only part to be estimated by the LMMSE process is $\sqrt{\frac{1}{1+K}}\mathbf{H}_{\text{RL}}$. Hence, the $\mathbf{R}_{\mathbf{H}}$ in (61) is replaced by $\frac{1}{1+K}\mathbb{E}[\mathbf{H}_{\text{RL}}\mathbf{H}_{\text{RL}}^H] = \frac{1}{1+K}\mathbf{I}$.

Therefore, we get $\mathbf{\Sigma} = \frac{1}{1+K+\Gamma_p}\mathbf{I}$ and

$$I_{\text{GMI}}(\Gamma) = \log\det\left(\mathbf{I} + \frac{\Gamma_d}{1+\frac{\Gamma_d}{1+K+\Gamma_p}}\hat{\mathbf{H}}\hat{\mathbf{H}}^H\right). \tag{66}$$

By defining

$$\psi_{\text{RC}}(\Gamma) \triangleq \frac{\Gamma_d}{1+\frac{\Gamma_d}{1+K+\Gamma_p}} = \frac{\kappa_d\Gamma(1+K+A_{\text{SP}}^2\kappa_d\Gamma)}{1+K+(1+A_{\text{SP}}^2)\kappa_d\Gamma}, \tag{67}$$

(66) can be rewritten by $I_{\text{GMI}}(\Gamma) = \mathcal{I}_o(\psi_{\text{RC}}(\Gamma), \hat{\mathbf{H}})$, whose ergodic Jensen approximation $\tilde{I}_{\text{GMI}}(\Gamma) = \mathbb{E}_{\hat{\mathbf{H}}}[I_{\text{GMI}}(\Gamma)]$ can be approximated by $\tilde{I}_{\text{GMI}}(\Gamma) \approx \log(\nu_{\text{RC}}(\psi_{\text{RC}}(\Gamma))) \triangleq \hat{I}_{\text{GMI}}(\Gamma)$ for $\Gamma \gg 1$.

The rest of the derivation resembles that of Section VI-A.2. The ζ in (12) is extracted from $\nu_{\text{RC}}(\zeta) = \mathcal{E}_R$, which originates in $\hat{I}_{\text{SISO}}(\Gamma') = 2C_{\text{SISO}}$ and $\zeta = \psi_{\text{RC}}(\Gamma')$. The scaling factor $\epsilon(\cdot)$ is numerically identified to ensure $\hat{I}_{\text{GMI}}(\psi_{\text{RC}}^{-1}(\zeta')) = \mathbb{E}_{\hat{\mathbf{H}}}[I_{\text{GMI}}(\psi_{\text{RC}}^{-1}(\epsilon(\zeta')\zeta'))]$, particularly in the form of $f_{\text{co}}^{\text{RC|CE}}(\zeta'_{\text{dB}}|\Theta_{\text{XPD}})$ in (35). Given the corrected surrogate $\hat{\zeta} = \epsilon(\zeta)\zeta$ in (34), projecting $\hat{\zeta}$ back to the Γ-domain by $\psi_{\text{RC}}^{-1}(\hat{\zeta})$ yields the final estimate τ_{M} in (33), which concludes the derivation. □

B. Derivation of Result 5: Class E, Layered MIMO CL

This scenario can be understood as a combination of the approaches in Sections V-B and VI-A. Basically, the results are developed based on (68), as shown at the bottom of the next page, which presents the achievable rate of CL in terms of GMI.

1) Derivation of Result 5-1 (AWGN): In the AWGN case, the ergodic GMI reduces into

$$\begin{aligned}\mathbb{E}_{\hat{\mathbf{H}}}[I_{\text{GMI}}^{\text{CL}}(\Gamma)] &= I_{\text{GMI}}^{\text{CL}}(\Gamma)\\ &= \log\nu_{\text{AWGN}}(\Gamma_d) - \log\nu_{\text{AWGN}}(\Delta_{\text{LDM}}\Gamma_d),\end{aligned} \tag{69}$$

which corresponds to the result of Section V-B.1 with the substitution $\Gamma \to \Gamma_d$. Therefore, the resulting τ_{M} in this scenario is a scaled version of that of Section V-B.1 by a factor of $1/\kappa_d$. □

2) Derivation of Result 5-2 (RL): The RL instance observes (68) to be rewritten by

$$I_{\text{GMI}}^{\text{CL}}(\Gamma) = q_{\hat{\mathbf{H}}}(\psi_{\text{RL}}(\Gamma)) - q_{\hat{\mathbf{H}}}(\Delta_{\text{LDM}}\psi_{\text{RL}}(\Gamma)), \tag{70}$$

[13]See [1], Annex A, which shows that the τ_{S} values of our interest are not particularly low.

$$\begin{aligned}\mathbb{E}_{\hat{\mathbf{H}}}[I_{\text{GMI}}(\Gamma)] \le \tilde{I}_{\text{GMI}}(\Gamma) &= \log\mathbb{E}_{\hat{\mathbf{H}}}\left[1 + \frac{\Gamma_d}{1+\frac{\Gamma_d}{1+\Gamma_p}}\sum_{i,j}|\hat{h}_{ij}|^2 + \left(\frac{\Gamma_d}{1+\frac{\Gamma_d}{1+\Gamma_p}}\right)^2|\hat{h}_{00}\hat{h}_{11} - \hat{h}_{10}^*\hat{h}_{01}^*|^2\right]\\ &= \log\left(1 + \frac{2\Gamma_d\Gamma_p}{1+\Gamma_d+\Gamma_p} + \frac{(2\Omega_{\text{RL}}\Gamma_p^2+2\Gamma_p+1)\Gamma_d^2\Gamma_p^2}{2(1+\Gamma_d+\Gamma_p)^2(1+\Gamma_p)^2}\right)\end{aligned} \tag{62}$$

where

$$q_{\hat{\mathbf{H}}}(\gamma) \triangleq \log\left(1+\gamma\sum_{i,j}\left|\hat{h}_{ij}\right|^2+\gamma^2\left|\hat{h}_{00}\hat{h}_{11}-\hat{h}_{10}^*\hat{h}_{01}^*\right|^2\right).$$

The statistical properties of $\hat{\mathbf{H}}$ and $\tilde{\mathbf{H}}$ are the same as those described in Section VI-A.2. Accordingly, the Jensen approximation of $\mathbb{E}_{\hat{\mathbf{H}}}[I_{\text{GMI}}^{\text{CL}}(\Gamma)]$ is cast as $\tilde{I}_{\text{GMI}}^{\text{CL}}(\Gamma) = \log \nu_{\text{RL}}\left(\frac{(1+\Gamma_p)\Gamma_d}{1+\Gamma_d+\Gamma_p}\right) - \log \nu_{\text{RL}}\left(\frac{\Delta_{\text{LDM}}(1+\Gamma_p)\Gamma_d}{1+\Gamma_d+\Gamma_p}\right)$. For high Γ, this can be further approximated by

$$\hat{I}_{\text{GMI}}^{\text{CL}}(\Gamma) = \log \nu_{\text{RL}}(\psi_{\text{RL}}(\Gamma)) - \log \nu_{\text{RL}}(\Delta_{\text{LDM}}\psi_{\text{RL}}(\Gamma)) \tag{71}$$

with $\nu_\mu(\cdot)$ given in (64) and $\psi_{\text{RL}}(\cdot)$ in (65).

For brevity, we define the domain transformation $\mathcal{T}_\psi : \psi_{\text{RL}}(\gamma) \mapsto \gamma$, such that $(\mathcal{T}_\psi f)(\psi_{\text{RL}}(\gamma)) = f(\gamma)$. Using this transformation, we introduce the auxiliary notations for $\hat{I}_{\text{GMI}}^{\text{CL}}$ and $\mathbb{E}_{\hat{\mathbf{H}}}[I_{\text{GMI}}^{\text{CL}}]$ as

$$\begin{aligned} L &\triangleq \mathcal{T}_\psi\left\{\hat{I}_{\text{GMI}}^{\text{CL}}\right\} && \text{s.t.} \quad L(\psi_{\text{RL}}(\gamma)) = \hat{I}_{\text{GMI}}^{\text{CL}}(\gamma), \\ L_E &\triangleq \mathcal{T}_\psi\left\{\mathbb{E}_{\hat{\mathbf{H}}}\left[I_{\text{GMI}}^{\text{CL}}\right]\right\} && \text{s.t.} \quad L_E(\psi_{\text{RL}}(\gamma)) = \mathbb{E}_{\hat{\mathbf{H}}}\left[I_{\text{GMI}}^{\text{CL}}(\gamma)\right]. \end{aligned}$$

In the ψ-transformed domain, ζ_c is defined as the solution of $L(\zeta_c) = 2C_{\text{SISO}}$, which is equivalent to $\hat{I}_{\text{GMI}}^{\text{CL}}\psi_{\text{RL}}^{-1}(\zeta_c) = 2C_{\text{SISO}}$. Precisely, the ζ_c expression in (26) is extracted from

$$\frac{1+2\zeta_c+\Omega_{\text{RL}}\zeta_c^2}{1+2\Delta_{\text{LDM}}\zeta_c+\Omega_{\text{RL}}\Delta_{\text{LDM}}^2\zeta_c^2} = \mathcal{E}_R. \tag{72}$$

Again, Padé approximation of (70) yields $I_{\text{GMI}}^{\text{CL}}(\Gamma) \approx \log\det(\mathbf{I} + \Phi(\psi_{\text{RL}}(\Gamma))\hat{\mathbf{H}}\hat{\mathbf{H}}^H) = \mathcal{I}_o((\Phi\circ\psi_{\text{RL}})(\Gamma), \hat{\mathbf{H}})$. Simply, we obtain $L_E(\zeta_c) \approx \mathbb{E}_{\hat{\mathbf{H}}}[\mathcal{I}_o(\Phi(\zeta_c), \hat{\mathbf{H}})]$, which provides a link between ζ_c and $L(\zeta_c)$ to $L_E(\psi_{\text{RL}}^{-1}(\tau_{\text{M}}))$, as established in Section V-B.2. The mapping $\mathcal{M}$ defined in Section V-B.2,

$$\mathcal{M} : L \mapsto \tilde{K} \quad \text{s.t.} \quad L(\omega) = \tilde{K}(\Phi(\omega)), \tag{73}$$

defines $\tilde{K}(\cdot)$, the projection of $L(\cdot)$ onto the $\Phi(\Gamma)$ domain. This mapping also transforms $L_E(\cdot)$ into $K_E(\cdot)$ as

$$\mathcal{M} : L_E \mapsto K_E \quad \text{s.t.} \quad L_E(\omega) = K_E(\Phi(\omega)). \tag{74}$$

On the domain of $\zeta_{\text{CL}} \triangleq \Phi(\zeta_c)$, we recall the correction function $\epsilon(\cdot)$ obtained in Section VI-A.2, which gives $\tilde{\mathcal{I}}_o(\zeta_{\text{CL}}, \hat{\mathcal{H}}) = K_E(\epsilon(\zeta_{\text{CL}})\zeta_{\text{CL}})$ based on the Padé approximation above. Here, $\tilde{\mathcal{I}}_o(\cdot)$ references (59) and $\hat{\mathcal{H}}$ denotes the ensemble set of $\hat{\mathbf{H}}$. Approximating $\tilde{K}(\zeta_{\text{CL}}) \approx \tilde{\mathcal{I}}_o(\zeta_{\text{CL}}, \hat{\mathcal{H}})$ then brings $\hat{\zeta}_{\text{CL}} = \epsilon(\zeta_{\text{CL}})\zeta_{\text{CL}}$, where $\epsilon(\cdot)$ references $f_{\text{co}}^{\text{RL}|\text{CE}}(\zeta_{\text{CL}}^{\text{dB}}|\Theta_{\text{XPD}})$ in (31).

Having determined ζ_c and obtained $\hat{\zeta}_{\text{CL}}$, the remaining step is to apply the reverse projections through $\Phi^{-1}(\cdot)$ and $\psi_{\text{RL}}^{-1}(\cdot)$. Specifically, $\zeta_r = \Phi^{-1}(\hat{\zeta}_{\text{CL}})$ and $\tau_{\text{M}}^{\text{CL}} = \psi_{\text{RL}}^{-1}(\zeta_r)$ direct to (38) and (37), respectively, by solving the equations $\Phi(\zeta_r) = \hat{\zeta}_{\text{CL}}$ and $\psi_{\text{RL}}(\tau_{\text{M}}^{\text{CL}}) = \zeta_r$, with reference to (25) and (65). □

3) Derivation of Result 5-3 (RC): Repeating the procedure in Section VI-B.2, using the properties of Section VI-A.3, readily leads to *Result 9*. □

C. Derivation of Result 6: Class E, Layered MIMO EL

Unlike the Class P case in Section V-C, CSIR error leaves a residual signal after SIC, often termed cross-layer interference (CLI). Such a conservative model accounting for CLI yields the signal expression (6) and leads to the GMI

$$\begin{aligned} I_{\text{GMI}}^{\text{EL}}(\Gamma) &= \log\det\left(\mathbf{I} + \Delta_{\text{LDM}}\Gamma_d\hat{\mathbf{H}}^H(\mathbf{I}+\Gamma_d\boldsymbol{\Sigma})^{-1}\hat{\mathbf{H}}\right) \\ &= \log\det\left(\mathbf{I} + \Delta_{\text{LDM}}\psi_\mu^o(\Gamma)\hat{\mathbf{H}}\hat{\mathbf{H}}^H\right), \end{aligned} \tag{75}$$

where $\psi_\mu^o(\Gamma)$ is given by $\psi_{\text{AWGN}}^o(\Gamma) = \Gamma_d$, $\psi_{\text{RL}}^o(\Gamma) = \Gamma_d(1+\Gamma_d(1+\Gamma_p)^{-1})^{-1}$, and $\psi_{\text{RC}}^o(\Gamma) = \psi_{\text{RC}}(\Gamma)$. Note that $\psi_\mu^o(\Gamma)$ is introduced to express $\psi_{\text{RL}}^o(\Gamma)$ in (75), which is slightly different from $\psi_{\text{RL}}(\Gamma)$ used in the subsequent approximation. Hence, the EL case can be handled by the same procedure as the SL case in Section VI-A, with the substitution $\Gamma \to \Delta_{\text{LDM}}\psi_\mu^o(\Gamma)$. For the ergodic version of (75), the Jensen approximation is first obtained as $\tilde{I}_{\text{GMI}}^{\text{EL}}(\Gamma) = \log\mathbb{E}_{\hat{\mathbf{H}}}\left[\det\left(\mathbf{I}+\Delta_{\text{LDM}}\psi_\mu^o(\Gamma)\hat{\mathbf{H}}\hat{\mathbf{H}}^H\right)\right]$, which admits the high-$\Gamma$ approximation

$$\hat{I}_{\text{GMI}}^{\text{EL}}(\Gamma) = \log \nu_\mu(\Delta_{\text{LDM}}\psi_\mu(\Gamma)). \tag{76}$$

Here, $\psi_{\text{AWGN}}(\Gamma) \triangleq \Gamma$. The definition of ζ in Section IV-C follows from $\nu_\mu(\zeta) = \mathcal{E}_R$, which is equivalent to the condition $\hat{I}_{\text{GMI}}^{\text{EL}}(\psi_\mu^{-1}(\zeta)) = 2C_{\text{SISO}}$. The approximation gap is then corrected by applying $f_{\text{co}}^{\mu|\text{CE}}(\zeta_{\text{dB}}|\Theta_{\text{XPD}})$ to produce $\zeta_{\text{EL}} = \epsilon(\zeta)\zeta/\Delta_{\text{LDM}}$ in (45). As defined in the previous sections, $\epsilon(\cdot)$ is the linear-scale form of $f_{\text{co}}^{\mu|\text{CE}}(\cdot)$. Overall, $\zeta_{\text{EL}} \approx \psi_\mu(\tau_{\text{M}}^{\text{EL}})$.

Due to CLI, the ToV estimate is no longer a direct amplification by $1/\Delta_{\text{LDM}}$ of the τ_{M} results for the SL case; such amplification is instead handled in the ζ-domain, which is the ψ_μ-transformed domain of Γ. The final estimate $\tau_{\text{M}}^{\text{EL}}$ is obtained after projecting back to the Γ-domain, i.e., by inverting ψ_μ as $\tau_{\text{M}}^{\text{EL}} = \psi_\mu^{-1}(\zeta_{\text{EL}})$. The inversion of $\psi_\mu(\cdot)$ is carried out by solving quadratic equations, which yields (42)-(44). □

VII. Remark: Channel XPD and Antenna XPD

The term *channel XPD*, represented by χ_L^{dB} and χ_N^{dB}, is clarified to avoid ambiguity. Cross-polarization antennas often specify XPD values in product datasheets, which characterize output *leakage* crossing over polarizations. To distinguish this property from channel XPD, we specifically refer to it as *antenna XPD*.

In fact, antenna XPD contributes directly to channel XPD. This antenna impairment, combined with over-the-air effects, results in the channel XPD. Let χ_{TA}^{dB} and χ_{RA}^{dB} denote the dB-scale antenna XPD measured at the transmit and receive antennas, respectively, and let $r \in [0, 1]$ denote the fraction of polarization-shifted signal power within the reflected signal waves during propagation. Defining $e_T \triangleq 10^{-\frac{\chi_{TA}^{\text{dB}}}{10}}$ and $e_R \triangleq 10^{-\frac{\chi_{RA}^{\text{dB}}}{10}}$, the channel XPDs can be determined by

$$\begin{aligned} \chi_L &= \left(\frac{1+\sqrt{e_R e_T}}{\sqrt{e_R}+\sqrt{e_T}}\right)^2, \\ \chi_N &= \frac{1+e_R e_T-(1-e_R-e_T+e_R e_T)r}{e_R+e_T+(1-e_R-e_T+e_R e_T)r}, \end{aligned} \tag{77}$$

$$I_{\text{GMI}}^{\text{CL}}(\Gamma) = \log\det(\mathbf{I}+\Gamma_d\boldsymbol{\Sigma}+\Gamma_d\hat{\mathbf{H}}\hat{\mathbf{H}}^H) - \log\det(\mathbf{I}+\Gamma_d\boldsymbol{\Sigma}+\Delta_{\text{LDM}}\Gamma_d\hat{\mathbf{H}}\hat{\mathbf{H}}^H) \tag{68}$$

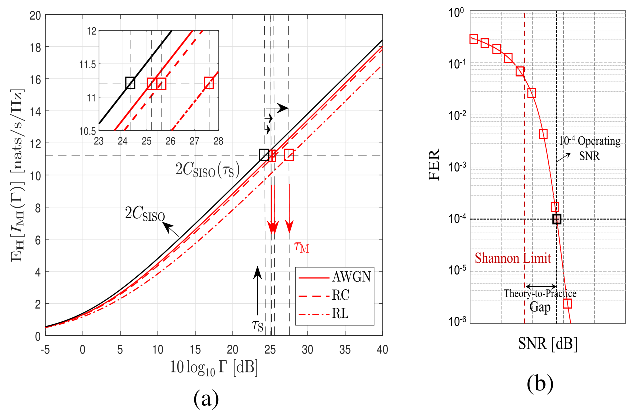

Fig. 2. (a) Abstraction of capacity matching ($\chi_L^{\text{dB}} = 10$ dB, $\chi_N^{\text{dB}} = 0$ dB); (b) Schematic illustration of FEC code performance vs. Shannon limit.

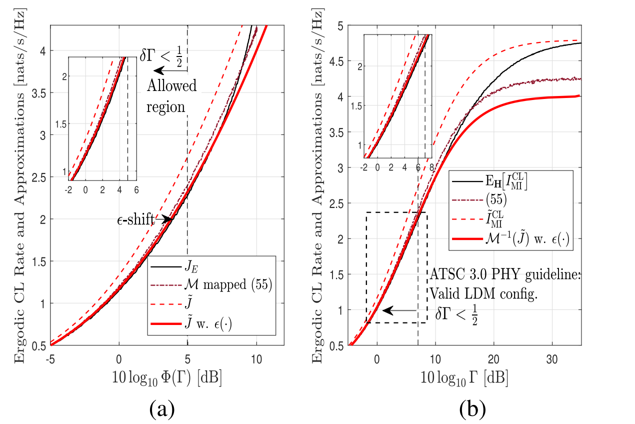

Fig. 3. Ergodic CL rate and the approximations over (a) $\Phi(\Gamma)$ domain and (b) Γ domain (μ = RL, $\delta = 0.1$ ($\mathtt{IL}$ = 10 dB), $\chi_N^{\text{dB}} = 10$ dB).

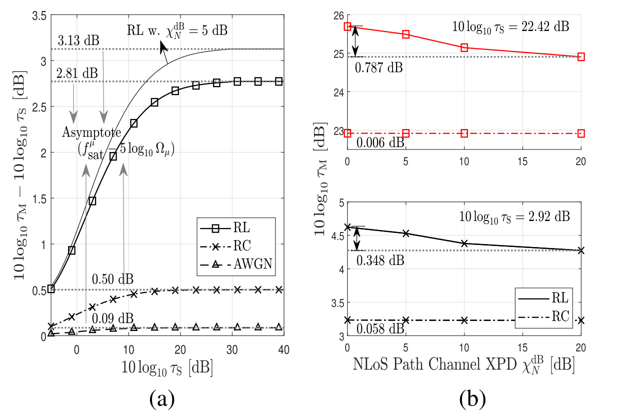

Fig. 4. (a) ToV penalty from τ_S (Class P, $\chi_L^{\text{dB}} = 20$ dB, $\chi_N^{\text{dB}} = 10$ dB), (b) τ_M vs. χ_N^{dB} (Class P, $\chi_L^{\text{dB}} = 20$ dB).

where $\chi_L^{\text{dB}} = 10\log_{10}\chi_L$ and $\chi_N^{\text{dB}} = 10\log_{10}\chi_N$ denote their dB-scale forms.

§ *Remark: Effective XPD*

In practice, field measurements may not distinguish the LoS and NLoS contributions separately. The XPD observed by practitioners would therefore reflect a comprehensive mix of both, namely, the *effective XPD*. Exhibiting the relationship among χ_L, χ_N, and the effective XPD, the effective XPD is given by

$$\chi_{\text{eff}} = \frac{\rho_L K + \rho_N}{(1-\rho_L)K + 1 - \rho_N} = \frac{\chi_L(1+\chi_N)L + \chi_N(1+\chi_L)}{(1+\chi_N)K + 1 + \chi_L} \tag{78}$$

in a generalized form. The AWGN and RL cases arise as special cases of (78), corresponding to $K \to \infty$ and $K = 0$, respectively. □

VIII. Numerical Results

This section presents numerical analyses of the proposed *ToV Estimators*. The framework is first examined using the derived models, followed by verifications through comparisons with link-level simulations.

A. Analysis on Capacity Matching and Approximations

Overall, *ToV Estimators* rely on the matching of MI metrics, shortly called a *capacity matching*. The fundamental mechanism of this scheme is abstracted in Fig. 2(a), with Monte Carlo-computed $\mathbb{E}_\mathbf{H}[I_\text{MI}(\Gamma)]$s. Given τ_S for the target BICM (presumably together with other setups such as time/frequency interleaving and fast Fourier transform (FFT)), double SISO capacity $2C_\text{SISO}$ is computed. The procedure then moves *horizontally* to spot $\mathbb{E}_\mathbf{H}[I_\text{MI}]$ at the same level, and τ_M is found by casting back the mapping. Since the ergodic realization depends on channel statistics, the resulting τ_M varies accordingly.

In practice, such an information-theoretic approach may exhibit a gap compared with real systems due to the performance loss inherent in practical coding schemes. However, state-of-the-art (SOTA) forward error correction (FEC) designs, such as the LDPC codes adopted in ATSC 3.0 and 3GPP 5G, are known as Shannon-approaching codes, achieving less than 0.5 dB gap. In particular, [59], [60], [61] report that ATSC 3.0 BICMs achieve a gap of 0.41 ~ 0.73 dB between FER = 10^{-4} and the Shannon limit.[14] This observation validates the use of the proposed *ToV Estimators* for SOTA MIMO broadcasting systems such as ATSC3.0 MIMO.

In addition, extending from Section V-B.2, the approximations for LDM-case estimations are numerically validated. ATSC 3.0 recommends choosing physical-layer parameters satisfying $\delta\tau_\text{S} < \frac{1}{2}$, presumably $\delta\tau_\text{M} < \frac{1}{2}$ when it comes to MIMO. Fig. 3 shows that the approximation ϵ-shifted $\tilde{I}_\text{MI}^\text{CL}$ aligns with the objective $\mathbb{E}_\mathbf{H}[I_\text{MI}^\text{CL}]$. Fig. 3(a) demonstrates the alignment in the $\mathcal{M}$-mapped space, and the corresponding Γ-domain translation is depicted in Fig. 3(b). Note in Fig. 3 that only the regions $\Gamma < 7$ dB and $\Phi(\Gamma) < 4.9556$ dB are physically valid according to A/327. Within these regions, the ϵ-shifted $\tilde{J}$ aligns well with J_E, thereby validating the approximation of $\mathbb{E}_\mathbf{H}[I_\text{MI}^\text{CL}(\Gamma)]$.

B. Impact of XPD and Asymptotic Properties

Fig. 4(a) illustrates the ToV penalty $10\log_{10}\tau_\text{M} - 10\log_{10}\tau_\text{S}$, for which XPD is particularly responsible. Giving

[14]Under quadrature phase shift keying (QPSK), AWGN channel, and sum-product algorithm (SPA) decoding.

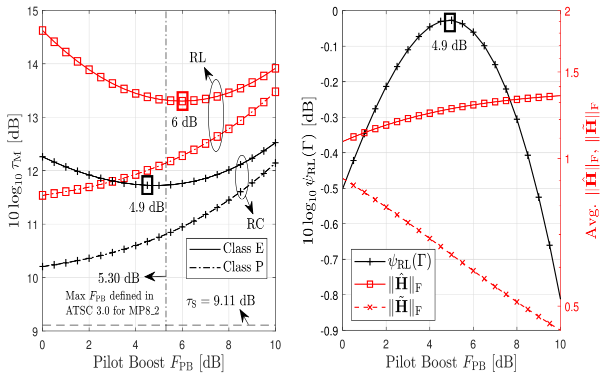

(a) (b)

Fig. 5. Effect of pilot boosting: (a) $\tau_{\rm M}$ vs. $F_{\rm PB}$ ($\tau_{\rm S}$ = 9.11 dB, $\chi_L^{\rm dB}$ = 10 dB, $\chi_N^{\rm dB}$ = 5 dB), (b) $\psi_{\rm RL}(\Gamma)$, $\mathbb{E}_{\mathbf{H}}\big[\|\hat{\mathbf{H}}\|_{\rm F}\big]$, $\mathbb{E}_{\mathbf{H}}\big[\|\tilde{\mathbf{H}}\|_{\rm F}\big]$ vs. $F_{\rm PB}$ (Class E, μ = RL, Γ = 1.5 dB, $\chi_N^{\rm dB}$ = 5 dB).

opportunities for a further rough guess of $\tau_{\rm M}$, the penalty is also shown to converge to the upper bound asymptotically. This behavior is readily deduced from (12) by *Corollary 1.1*, giving a handy asymptote for Class P SL estimates:

$$10\log_{10}\tau_{\rm M} \underset{\tau_{\rm S}\gg 1}{\longrightarrow} 10\log_{10}\frac{\tau_{\rm S}}{\sqrt{\Omega_\mu}} + f_{\rm sat}^{\mu}.$$

It follows that the ToV penalty is upper-bounded by the asymptote ToV Increase [dB] $\longrightarrow f_{\rm sat}^{\mu} - 5\log_{10}\Omega_\mu$. When it comes to the Class E case (see *Corollary 4.1*), a similar applies to $\psi_\mu(\Gamma)$; a markup $\frac{1+A_{\rm SP}^2}{A_{\rm SP}^2\kappa_d}$ appears in $\tau_{\rm M}$, leading to ToV Increase [dB] $\longrightarrow 10\log_{10}\frac{1+A_{\rm SP}^2}{A_{\rm SP}^2\kappa_d} + f_{\rm sat}^{\mu} - 5\log_{10}\Omega_\mu$.

It is observed that the ToV penalty increases as the NLoS XPI appears significant. This trend is shown in Fig. 4(a), where the penalty is largest for RL, followed by RC and AWGN. 4(b) further demonstrates a pronounced deviation in the RL case with respect to XPD, whereas the RC case exhibits minor variation. In addition, results also show that the XPI impact, in terms of $\tau_{\rm M}$ degradation, arises more significantly at higher operating CNR, equivalently, higher $\tau_{\rm S}$.

C. Pilot Boosting Effect

The tradeoff between data signal quality and channel estimation accuracy can be clearly observed through the Class E model. Obviously, pilot boosting always increases $\tau_{\rm M}$ (degrades reception) under the Class P model, since perfect CSIR is already assumed regardless of training signal distortion. By contrast, Class E reflects the benefit of improved channel estimation accuracy. This aspect is illustrated in Fig. 5(a). In both RL and RC plots for the Class E results, convex-like tradeoff curves are explicitly observed. The optimal pilot boosting level that minimizes $\tau_{\rm M}$ is identified as 6.0 dB for the RL channel and 4.9 dB for the RC channel. Note that the maximum pilot boosting level allowed in ATSC 3.0 for pilot pattern MP8_2 is 5.30 dB[15]; thus, 6.0 dB lies outside this range, whereas 4.9 dB lies within it. Hence, in this example, the optimal $F_{\rm PB}$ for the RL case is 5.3 dB.

Fig. 5(b) further delves into the tradeoff by probing the effective signal power and channel estimation accuracy. Specifically, $\mathbb{E}_{\mathbf{H}}\big[\|\hat{\mathbf{H}}\|_{\rm F}\big]$ strictly increases over $F_{\rm PB}$ (equivalently, $\mathbb{E}_{\mathbf{H}}\big[\|\tilde{\mathbf{H}}\|_{\rm F}\big]$ decreases), while $\psi_{\rm RL}(\Gamma)$ exhibits concavity. The combination of monotonically increasing $\mathbb{E}_{\mathbf{H}}\big[\|\hat{\mathbf{H}}\|_{\rm F}\big]$ and concave $\psi_{\rm RL}$ produces the behavior of $\tau_{\rm M}$ found in Fig. 5(a).

D. Examination: Comparison With Link-Level Simulations

A confirmatory experiment is carried out through link-level simulations. To this end, an extensive end-to-end simulator was implemented, incorporating the entire ATSC 3.0 physical layer with the newly adopted *MIMO Extension* [2], [21]. This simulator builds upon the platform used in [28], whose results were officially incorporated into A/327.

In particular, the physical-layer configurations listed in Table XI were used. A total of eight configuration sets were tested: six SL configurations and two layered MIMO sets, each with a different ModCod combination and the corresponding $\tau_{\rm S}$. The $\tau_{\rm S}$ values are referenced from A/327 Annex A, which specifies the QEF criterion at FER = 10^{-4}. Consistently, the $\tau_{\rm M}$ estimates inherit this QEF condition applied to $\tau_{\rm S}$; the simulations were likewise conducted at FER = 10^{-4}. This FER was measured after LDPC decoding, where all test configurations employed a BCH outer code; that is, the BCH+LDPC option was used in the concatenated coding format of ATSC 3.0. Specifically, LDPC codes of length 64,800 bits were used. For decoding, the SPA was employed for LDPC decoding, allowing up to 50 iterations. The ToV measurements were obtained with a 0.1-dB step size, implying a possible measurement error of $\pm$ 0.1 dB.

Throughout all simulation scenarios, the system employed a 16K-size FFT and convolutional time interleaving (CTI) with a depth of 1024 samples. To be noticed, the aforementioned setting is consistent with that used for $\tau_{\rm S}$ measurements [1], [28]. In what follows, the simulation outcomes are referred to as *measured*, and those from the proposed *ToV Estimators* as *estimated*.

All tests were conducted under XPD = 20 dB, which has been used as a baseline profile in Brazilian TV 3.0 activities: i.e., $\chi_L^{\rm dB}$ = 20 dB or $\chi_N^{\rm dB}$ = 20 dB when available, depending on μ. To comply with convention standards, RL20 (DVB-P1) and RC20 (DVB-F1) channel models were used for the RL and RC environments, respectively. Note that we resorted to those standard SISO multipath models by replicating the same multipath profile across all inter-antenna paths, e.g., *pol* #1-to-*pol* #1, *pol* #1-to-*pol* #2, etc. This figure may deviate from the uncorrelated property of NLoS channel entries, but it nonetheless offers useful and insightful results that can guide the practice.

The simulations employed perfect channel estimation,[16] and, accordingly, Class P procedure is applied to derive the estimates. A scattered pilot pattern MP8_2 was used with no

[15]The options of boosting level are defined differently according to the pilot pattern. According to A/322 support, the effective factor $\frac{A_{\rm SP}^2}{D_X D_Y}$ ranges $-21.07 \sim -4.88$ dB.

[16]This refers to the setup in which the receiver channel estimator treats every OFDM cell as a pilot. While this is fundamentally different from assuming perfect CSIR, in stationary channel scenarios it is effectively equivalent to perfect CSIR.

TABLE XI
TEST CONFIGURATIONS: ATSC 3.0 PHYSICAL LAYER PARAMETERS

Bandwidth / Occupied Bandwidth	6 MHz / 5.832844 MHz
FFT Size	16K
Guard Interval Duration	111.11 μs (GI4_768)
Pilot Encoding / Pilot Pattern	Null Pilot Encoding / MP8_2 ($D_X = 8$, $D_Y = 2$)

Test Scenario (Simulation, SL)		$\mathcal{SC}_{S1}$	$\mathcal{SC}_{S2}$	$\mathcal{SC}_{S3}$	$\mathcal{SC}_{S4}$	$\mathcal{SC}_{S5}$	$\mathcal{SC}_{S6}$
PLP Identifier		$\mathcal{P}_{\mathsf{SimS1}}$	$\mathcal{P}_{\mathsf{SimS2}}$	$\mathcal{P}_{\mathsf{SimS3}}$	$\mathcal{P}_{\mathsf{SimS4}}$	$\mathcal{P}_{\mathsf{SimS5}}$	$\mathcal{P}_{\mathsf{SimS6}}$
PLP Layer		SL (Non-LDM)					
Payload BICM	Inner Code (LDPC)	8/15	5/15	6/15	8/15	5/15	7/15
	Constellation	QPSK	16 NUC	16 NUC	16 NUC	64 NUC	64 NUC
Reference ToV τ_{S} [28], [1]		1.32 dB	2.92 dB	4.41 dB	6.52 dB	6.12 dB	9.11 dB

Test Scenario (Simulation, LDM)		$\mathcal{SC}_{L1}$		$\mathcal{SC}_{L2}$	
PLP Identifier		$\mathcal{P}_{\mathsf{CL,\,SimL1}}$	$\mathcal{P}_{\mathsf{EL,\,SimL1}}$	$\mathcal{P}_{\mathsf{CL,\,SimL2}}$	$\mathcal{P}_{\mathsf{EL,\,SimL2}}$
PLP Layer		LDM CL	LDM EL	LDM CL	LDM EL
Injection Level $10\log_{10}\delta$		N/A	-10 dB	N/A	-16 dB
Payload BICM	Inner Code	6/15 LDPC	5/15 LDPC	7/15 LDPC	5/15 LDPC
	Constellation	16 NUC	16 NUC	64 NUC	16 NUC
Reference ToV (SL) τ_{S}		4.41 dB	2.92 dB	9.11 dB	2.92 dB

TABLE XII
TEST RESULTS: SL SIMULATIONS (XPD = 20 dB)

		Sim. Meas. [dB]	Class P Estimate [dB]	Diff.
$\mathcal{P}_{\mathsf{SimS1}}$	AWGN	1.4	1.37	0.03
	RL	3.1	2.48	0.62
	RC	1.6	1.59	0.01
$\mathcal{P}_{\mathsf{SimS2}}$	AWGN	3.0	2.98	0.02
	RL	4.3	4.27	0.03
	RC	3.2	3.22	0.02
$\mathcal{P}_{\mathsf{SimS3}}$	AWGN	4.5	4.47	0.03
	RL	6.1	5.93	0.17
	RC	4.8	4.75	0.05
$\mathcal{P}_{\mathsf{SimS4}}$	AWGN	6.6	6.59	0.01
	RL	8.6	8.26	0.34
	RC	6.9	6.91	0.01
$\mathcal{P}_{\mathsf{SimS5}}$	AWGN	6.2	6.19	0.01
	RL	7.8	7.82	0.02
	RC	6.5	6.50	0.00
$\mathcal{P}_{\mathsf{SimS6}}$	AWGN	9.2	9.19	0.01
	RL	11.1	11.08	0.02
	RC	9.5	9.54	0.04

TABLE XIII
TEST RESULTS: LDM SIMULATIONS (XPD = 20 dB)

		Sim. Meas. [dB]	Class P Estimate [dB]	Diff.
$\mathcal{P}_{\mathsf{CL,SimL1}}$	AWGN	6.29 [17]	6.27	0.02
	RL	10.1	8.45	1.65
	RC	6.8	6.66	0.14
$\mathcal{P}_{\mathsf{EL,SimL1}}$	AWGN	13.42 [17]	13.48	0.06
	RL	14.8	14.74	0.06
	RC	13.7	13.72	0.02
$\mathcal{P}_{\mathsf{CL,SimL2}}$	AWGN	10.3	10.27	0.03
	RL	12.7	12.84	0.14
	RC	10.6	10.72	0.12
$\mathcal{P}_{\mathsf{EL,SimL2}}$	AWGN	19.2	19.17	0.03
	RL	20.5	20.43	0.07
	RC	19.5	19.42	0.08

pilot boosting (0 dB boost). Specifically, Table XI indicates that the null pilot encoding scheme was employed, while the performance with the Walsh–Hadamard scheme did not differ in these scenarios.

Table XII first addresses the SL configurations on the baseline. The simulation results are enumerated along with the estimate results. The deviations between measured and estimated results range from 0.00 dB to 0.62 dB; except for the $\mathcal{P}_{\mathsf{SimS1}}$ RL, $\mathcal{P}_{\mathsf{SimS3}}$ RL, and $\mathcal{P}_{\mathsf{SimS4}}$ RL cases, the gap remains mostly within 0.1 dB. One could recall that 6/15 code exhibits a notably larger gap from the Shannon limit compared to other coding options [59], and 8/15 code shows relatively greater AWGN-to-RL degradation compared to the trend [61]. These outliers are consistent with the fact that this work is grounded in an information-theoretic approach. Accordingly, when a particular code exhibits an atypically large implementation loss or deviates significantly from the theoretical baseline, the practical performance may be worse than the model's estimate. In contrast, for AWGN cases in Table XII, the estimates fall within 0.1 dB of the simulation results, which matches the simulation step resolution and demonstrates the high accuracy of *ToV Estimators*. The error standard deviation over Table XII results amounts to 0.16 dB.

Additionally, layered MIMO examples were evaluated. Both CL and EL PLPs were tested, with $\mathcal{P}_{\mathsf{CL,SimL1}}$ and $\mathcal{P}_{\mathsf{CL,SimL2}}$ corresponding to CL, and $\mathcal{P}_{\mathsf{EL,SimL1}}$ and $\mathcal{P}_{\mathsf{EL,SimL2}}$ corresponding to EL. The $\mathcal{P}_{\mathsf{CL,SimL1}}$ and $\mathcal{P}_{\mathsf{EL,SimL1}}$ measurements were adopted from [17]. As shown in Table XIII, the deviations between measured and estimated results range from 0.02 dB to 1.65 dB; except for the $\mathcal{P}_{\mathsf{CL,SimL1}}$ RL case, which is 1.65 dB, the gap remains mostly within 0.2 dB. It should again be noted that the 6/15-rate LDPC code in ATSC 3.0 has been reported to show an exceptionally large gap between the 10^{-4} FER point and the Shannon limit. Otherwise, the estimation errors fall within 0.2 dB, which is comparable to the simulation step size.

IX. CONCLUSION

This paper has presented compact closed-form methods for estimating the required CNR of dual-polarized MIMO broadcast systems under limited XPD. The proposed framework converts well-characterized SISO ToV data (e.g., A/327 Annex A) into MIMO ToV predictions for AWGN,

TABLE XIV
RMSE OF f_{co}^{μ}, $f_{\text{co}}^{\mu|\text{CE}}$

f_{co}^{μ}				$f_{\text{co}}^{\mu\|\text{CE}}$			
μ	Θ_{XPD}		RMSE	μ	Θ_{XPD}		RMSE
	χ_L^{dB}	χ_N^{dB}			χ_L^{dB}	χ_N^{dB}	
RL	-	20 dB	0.2684	RL	-	20 dB	0.3959
		10 dB	0.3403			10 dB	0.3339
		5 dB	0.2972			5 dB	0.3538
		0 dB	0.4671			0 dB	0.4682
RC	20 dB	20 dB	0.2802	RC	20 dB	20 dB	0.2591
		10 dB	0.2712			10 dB	0.2236
		5 dB	0.2619			5 dB	0.2449
		0 dB	0.2454			0 dB	0.2564
	10 dB	10 dB	0.2856		10 dB	10 dB	0.2665
		5 dB	0.2652			5 dB	0.2039
		0 dB	0.2804			0 dB	0.2169

RL, and RC channels, with explicit parameterization by channel XPD. Two estimator classes were developed: Class P (assuming perfect CSIR) and Class E (based on estimated CSIR). Both single-layer transmission and Layered MIMO Type A were addressed, and closed-form expressions were derived for CL and EL cases. The resulting estimators are lightweight, interpretable, and readily applicable to planning tools for coverage analysis, link budgeting, and interference studies.

APPENDIX A
RMSE OF f_{Co}^{μ} AND $f_{\text{Co}}^{\mu|\text{CE}}$: FITTING ALIGNMENT

The alignment of $f_{\text{co}}^{\mu}(\cdot)$ and $f_{\text{co}}^{\mu|\text{CE}}(\cdot)$ with the ground-truth $\epsilon(\cdot)$ data is assessed using the root mean square error (RMSE). The evaluated RMSE is shown in Table XIV.

APPENDIX B
ALTERNATIVE METHOD: A FURTHER NAIVE SHORTCUT

Although cruder, an alternative is to use the SISO ToV measurements obtained under channel-applied environments, instead of applying $f_{\text{co}}^{\mu}(\cdot)$ or $f_{\text{co}}^{\mu|\text{CE}}(\cdot)$ to address channel fading effects. As noted earlier, A/327 Annex A also reports measurement results under RL and RC channel conditions (specifically the RL20 and RC20 models). The simplest procedure used for the AWGN case can be directly applied to the RL or RC SISO ToV measurements. That is, the Class P procedure in Section III-A.1 and the Class E procedure in Section IV-A.1 can be applied to the results such as Tables A.3.3 and A.3.4 of A/327, while the counterparts in Sections III-B, IV-B.1, and IV-C can be used for LDM cases. This approach could provide a crude yet rapid guess, though lacking solid theoretical grounding.

ACKNOWLEDGMENT

This work is to be published in part by ATSC Doc. A/327 [1].

REFERENCES

[1] *Guidelines for the Physical Layer Protocol*, document A/327, Jul. 2025.
[2] *MIMO System Performance Estimation*, document A/327:2025-02, Jun. 2025.
[3] S. Ahn et al., "MIMO extension of ATSC 3.0: System design," *IEEE Trans. Broadcast.*, vol. 72, no. 2, Jun. 2026.
[4] D. Gómez-Barquero et al., "MIMO for ATSC 3.0," *IEEE Trans. Broadcast.*, vol. 62, no. 1, pp. 298–305, Mar. 2016.
[5] Z. H. Hong et al., "Frequency-domain RF self-interference cancellation for in-band full-duplex communications," *IEEE Trans. Wireless Commun.*, vol. 22, no. 4, pp. 2352–2363, Apr. 2023.
[6] Z. H. Hong et al., "Implementation of wireless backhaul and inter-tower communications with MIMO in ATSC 3.0," *IEEE Trans. Broadcast.*, vol. 69, no. 2, pp. 579–588, Jun. 2023.
[7] J. Kang, S.-I. Park, H. Jung, N. Hur, and S. Ahn, "Feasibility of backward compatible MIMO broadcasting: Issues in SISO-MIMO coexistence," *IEEE Trans. Broadcast.*, vol. 69, no. 2, pp. 589–609, Jun. 2023.
[8] E. Telatar, "Capacity of multi-antenna Gaussian channels," *Eur. Trans. Telecommun.*, vol. 10, pp. 585–598, Nov. 1999.
[9] D. E. Vargas Paredero, "Transmit and receive signal processing for MIMO terrestrial broadcast systems," Ph.D. thesis, Dept. Commun., Universitat Politecnica de Valencia, Valencia, Spain, May 2016.
[10] S. Ahn et al., "Converged distribution of 5G media: Opportunities of overlaid broadcast and emerging applications over dual connectivity," *IEEE Trans. Broadcast.*, vol. 68, no. 2, pp. 501–516, Jun. 2022.
[11] P. Siebert. (Jun. 3, 2019). *How DVB-T2 and ATSC 3.0 Stack Up: Technical Benefits, Limitations and Real-World Deployments*. Accessed: Sep. 8, 2025. [Online]. Available: https://www.tvtechnology.com/opinions/how-dvb-t2-and-atsc-3-0-stack-up-technical-benefits-limitations-and- real-world-deployments
[12] E. Dubs, "How IP-based broadcast meets 5G for resilient and sustainable media distribution," in *Proc. NAB Broadcast. Engin. Inform. Technol. (BEIT) Conf.*, 2024, pp. 1–24.
[13] J. Boyer et al., "*MIMO for broadcast–results from a high-power U.K. trial*," British Broadcast. Corporat., London, U.K., White Paper WHP 157, Oct. 2007.
[14] *TV 3.0 Project Website*. Accessed: Sep. 8, 2025. [Online]. Available: https://forumsbtvd.org.br/tv3_0/
[15] A. S. S. Chaubet et al., "TV 3.0: An overview," *IEEE Trans. Broadcast.*, vol. 71, no. 1, pp. 11–18, Mar. 2025.
[16] (2020). *Call for Proposals: TV 3.0 Project: SBTVD-T Forum*. [Online]. Available: https://forumsbtvd.org.br/wp-content/uploads/2020/07/SBTVDTV-3-0-CfP.pdf
[17] S. Ahn, B.-M. Lim, J. Kim, C. E. Cosme Ribeiro, L. Fausto, and S.-I. Park, "Geographic segmented localcasting based on LDM: Design and plans in Brazil," in *Proc. IEEE Int. Symp. Broadband Multimedia Syst. Broadcast. (BMSB)*, Jun. 2025, pp. 1–4.
[18] S. Ahn, S. Kwon, S.-K. Ahn, H. Jung, and S.-I. Park, "ATSC 3.0 for future broadcasting: Features and extensibility," *SET Int. J. BROADCAST Eng.*, vol. 6, pp. 22–36, Aug. 2020.
[19] S.-I. Park, B.-M. Lim, H. Jung, N. Hur, and S. Ahn, "Roads of MIMO broadcasting: An overview of variant technologies," *SET Int. J. Broadcast. Eng.*, vol. 9, pp. 57–59, Dec. 2023.
[20] *Physical Layer Protocol*, document A/322, Sep. 2024.
[21] *MIMO Extension*, document A/322:2024-04, Sep. 2024.
[22] E. Garro, C. Barjau, D. Gomez-Barquero, J. Kim, S.-I. Park, and N. Hur, "Layered division multiplexing with co-located multiple-input multiple-output schemes," *IEEE Trans. Broadcast.*, vol. 66, no. 1, pp. 9–20, Mar. 2020.
[23] H. Jung et al., "Feasibility verification of ATSC 3.0 MIMO system for 8K-UHD terrestrial broadcasting," *IEEE Trans. Broadcast.*, vol. 67, no. 4, pp. 909–916, Dec. 2021.
[24] (Jul. 2024). *TV 3.0 Project—Phase 3—Over-the-Air Physical Layer Field Tests: SBTVD-T Forum*. [Online]. Available: https://forumsbtvd.org.br/wpcontent/uploads/2024/07/SBTVD-TV_3_0-P3-PL-Field-Report.pdf
[25] (Nov. 2023). *TV 3.0 Project—Phase 3—Over-the-Air Physical Layer Laboratory Tests: SBTVD-T Forum*. [Online]. Available: https://forumsbtvd.org.br/wp-content/uploads/2023/11/SBTVD-TV_3_0-P3-PL-Lab-Report.pdf
[26] P. Kurz. (Aug. 27, 2025). *Brazil Makes It Official: New DTV+ Standard Leverages ATSC 3.0 Tech*. Accessed: Sep. 8, 2025. [Online]. Available: https://www.tvtechnology.com/news/brazil-makes-it-official-new-dtv-standard-leverages-atsc-3-0-tech
[27] (Aug. 2025). *Brazilian Presidential Decree, No. 12.595*. Accessed: Sep. 8, 2025. [Online]. Available: https://www2.camara.leg.br/legin/fed/decret/2025/decreto-12595-27-agosto-2025-797885-publicacaooriginal-176222-pe.html
[28] S.-I. Park et al., "Performance analysis of all modulation and code combinations in ATSC 3.0 physical layer protocol," *IEEE Trans. Broadcast.*, vol. 65, no. 2, pp. 197–210, Jun. 2019.
[29] S. Ahn et al., "Mobile performance evaluation for ATSC 3.0 physical layer modulation and code combinations under TU-6 channel," *IEEE Trans. Broadcast.*, vol. 66, no. 4, pp. 752–769, Dec. 2020.

[30] S. Ahn et al., "Characterization and modeling of UHF wireless channel in terrestrial SFN environments: Urban fading profiles," *IEEE Trans. Broadcast.*, vol. 68, no. 4, pp. 803–818, Dec. 2022.

[31] S. Ahn, B.-M. Lim, S. Kwon, S. Jeon, X. Wang, and S.-I. Park, "Diversity receiver for ATSC 3.0-in-vehicle: design and field evaluation in metropolitan SFN," *IEEE Trans. Broadcast.*, vol. 70, no. 2, pp. 367–381, Jun. 2024.

[32] B.-m. Lim et al., "Field evaluation of transmit diversity code filter sets in ATSC 3.0 single frequency networks," *IEEE Trans. Broadcast.*, vol. 68, no. 1, pp. 191–202, Mar. 2022.

[33] S.-K. Ahn et al., "Evaluation of ATSC 3.0 and 3GPP rel-17 5G broadcasting systems for mobile handheld applications," *IEEE Trans. Broadcast.*, vol. 69, no. 2, pp. 338–356, Jun. 2023.

[34] S. Kwon et al., "Comparative assessment of physical layer performance: ATSC 3.0 vs. 5G broadcast in laboratory and field tests," *IEEE Trans. Broadcast.*, vol. 71, no. 1, pp. 2–10, Mar. 2025.

[35] S. Ahn et al., "Probabilistic analysis on RF-watermark TxID detection in SFN with randomly distributed co-channel interferers and preamble cancellation," *IEEE Access*, vol. 8, pp. 56300–56311, 2020.

[36] S. Kwon, S.-I. Park, J.-Y. Lee, B.-M. Lim, S. Ahn, and J. Kang, "Detection schemes for ATSC 3.0 transmitter identification in single frequency network," *IEEE Trans. Broadcast.*, vol. 66, no. 2, pp. 229–240, Jun. 2020.

[37] K. P. Liolis, J. Gómez-Vilardebó, E. Casini, and A. I. Perez-Neira, "Statistical modeling of dual-polarized MIMO land mobile satellite channels," *IEEE Trans. Commun.*, vol. 58, no. 11, pp. 3077–3083, Nov. 2010.

[38] C. Oestges, B. Clerckx, M. Guillaud, and M. Debbah, "Dual-polarized wireless communications: From propagation models to system performance evaluation," *IEEE Trans. Wireless Commun.*, vol. 7, no. 10, pp. 4019–4031, Oct. 2008.

[39] P. Moss, "*2-by-2 MIMO fixed reception channel model for dual-polar terrestrial transmission*," British Broadcast. Corporat., London, U.K., White Paper WHP 161, 2008.

[40] (Dec. 2021). *Testing and Evaluation Report: TV 3.0 Project—Over-the-Air Physical Layer Laboratory Tests: SBTVD-T Forum*. [Online]. Available: https://forumsbtvd.org.br/wp-content/uploads/2021/12/SBTVD-TV_3_0-PLLab-Report.pdf

[41] (Dec. 2021). *Testing and Evaluation Report: TV 3.0 Project—Over-the-Air Physical Layer Field Tests: SBTVD-T Forum*. [Online]. Available: https://forumsbtvd.org.br/wp-content/uploads/2021/12/SBTVD-TV_3_0-PL-Field-Report.pdf

[42] B. Lim et al., "Unified SISO-MIMO transmission framework in ATSC 3.0: Design, implementation, and validation," *IEEE Trans. Broadcast*.

[43] R. S. Rabaça, G. H. M. G. D. Oliveira, L. N. D. S. Junior, P. B. Lopes, S.-I. Park, and C. Akamine, "Evaluation of ATSC 3.0 MODCODs for TV 3.0," in *Proc. IEEE Int. Symp. Broadband Multimedia Syst. Broadcast. (BMSB)*, Jun. 2024, pp. 1–5.

[44] S. Saito et al., "8K terrestrial transmission field tests using dual-polarized MIMO and higher-order modulation OFDM," *IEEE Trans. Broadcast.*, vol. 62, no. 1, pp. 306–315, Mar. 2016.

[45] H. Jung et al., "Impact of cross-polarization discrimination for ATSC 3.0 MIMO system," in *Proc. IEEE Int. Symp. Broadband Multimedia Syst. Broadcast. (BMSB)*, Aug. 2021, pp. 1–3.

[46] J.-Y. Lee et al., "Layered division multiplexing for ATSC 3.0: Implementation and memory use aspects," *IEEE Trans. Broadcast.*, vol. 65, no. 3, pp. 496–503, Sep. 2019.

[47] S. Ahn, S.-I. Park, J.-Y. Lee, N. Hur, and J. Kang, "Cooperation between LDM-based terrestrial broadcast and broadband unicast: On scalable video streaming applications," *IEEE Trans. Broadcast.*, vol. 67, no. 1, pp. 2–22, Mar. 2021.

[48] S. Ahn et al., "Large-scale network analysis on NOMA-aided broadcast/unicast joint transmission scenarios considering content popularity," *IEEE Trans. Broadcast.*, vol. 66, no. 4, pp. 770–785, Dec. 2020.

[49] S. Ahn, S.-I. Park, J.-Y. Lee, N. Hur, and J. Kang, "Fronthaul compression and precoding optimization for NOMA-based joint transmission of broadcast and unicast services in C-RAN," *IEEE Trans. Broadcast.*, vol. 66, no. 4, pp. 786–799, Dec. 2020.

[50] L. Zhang et al., "Layered-division-multiplexing: Theory and practice," *IEEE Trans. Broadcast.*, vol. 62, no. 1, pp. 216–232, Mar. 2016.

[51] E. Garro, J. J. Gimenez, S. I. Park, and D. Gomez-Barquero, "Scattered pilot performance and optimization for ATSC 3.0," *IEEE Trans. Broadcast.*, vol. 63, no. 1, pp. 282–292, Mar. 2017.

[52] J. Zhang, C.-K. Wen, S. Jin, X. Gao, and K.-K. Wong, "On capacity of large-scale MIMO multiple access channels with distributed sets of correlated antennas," *IEEE J. Sel. Areas Commun.*, vol. 31, no. 2, pp. 133–148, Feb. 2013.

[53] W. Hachem, O. Khorunzhiy, P. Loubaton, J. Najim, and L. Pastur, "A new approach for mutual information analysis of large dimensional multi-antenna channels," *IEEE Trans. Inf. Theory*, vol. 54, no. 9, pp. 3987–4004, Sep. 2008.

[54] H. Ju et al., "LDPC-coded LDM systems employing non-uniform injection level for combining broadcast and multicast/unicast services," *IEEE Trans. Broadcast.*, vol. 70, no. 3, pp. 1032–1043, Sep. 2024.

[55] A. Lapidoth and S. Shamai (Shitz), "Fading channels: How perfect need 'perfect side information' be?," *IEEE Trans. Inf. Theory*, vol. 48, no. 5, pp. 1118–1134, May 2002.

[56] T. Yoo and A. Goldsmith, "Capacity and power allocation for fading MIMO channels with channel estimation error," *IEEE Trans. Inf. Theory*, vol. 52, no. 5, pp. 2203–2214, May 2006.

[57] M. Medard, "The effect upon channel capacity in wireless communications of perfect and imperfect knowledge of the channel," *IEEE Trans. Inf. Theory*, vol. 46, no. 3, pp. 933–946, May 2000.

[58] M. Geller and E. W. Ng, "A table of integrals of the exponential integral," *J. Res. Nat. Bur. Standards, B. Math. Math. Sci.*, vol. 73B, no. 3, pp. 191–210, 1969.

[59] S. Myung, S.-I. Park, K.-J. Kim, J.-Y. Lee, S. Kwon, and J. Kim, "Offset and normalized min-sum algorithms for ATSC 3.0 LDPC decoder," *IEEE Trans. Broadcast.*, vol. 63, no. 4, pp. 734–739, Dec. 2017.

[60] K.-J. Kim et al., "Low-density parity-check codes for ATSC 3.0," *IEEE Trans. Broadcast.*, vol. 62, no. 1, pp. 189–196, Mar. 2016.

[61] F. Jerji and C. Akamine, "Advanced ISDB-T and ATSC 3.0 LDPC codes performance and complexity comparison," *IEEE Trans. Broadcast.*, vol. 68, no. 1, pp. 254–262, Mar. 2022.

Sungjun Ahn (Member, IEEE) received the B.S., M.S., and Ph.D. degrees in electrical engineering from Korea Advanced Institute of Science and Technology (KAIST) in 2015, 2017, and 2023, respectively. He has been with the Media Research Division, Electronics and Telecommunications Research Institute (ETRI) since 2017, where he is currently a Senior Research Engineer. He also served as a Research Fellow Board Member of ETRI from 2024 to 2025. He has authored more than 100 technical publications and holds more than 100 patents. He has contributed to ATSC 3.0 MIMO Extension standardization, particularly within ATSC S32, as well as to the standardization of Brazilian DTV+. His research group has worked on system design, field verification, standardization activities, and theoretical analyses for ATSC 3.0 digital terrestrial transmission and other wireless applications. He is currently involved in research on broadcasting-based terrestrial time transfer, MIMO broadcasting, multi-PHY coexistence, and semantic media systems and delivery protocols. He has received several honors and awards, including a Minister's Commendation from the Korean Minister of Science and ICT, the Young Researcher Award from ETRI, the Grand Prize of the Foundational Patent Award from ETRI, the Outstanding Ph.D. Dissertation Award from the College of Engineering, KAIST, and multiple Best Paper Awards from IEEE BMSB. He has also served as a Guest Editor for several special issues of IEEE TRANSACTIONS ON BROADCASTING.

Sung-Ik Park (Fellow, IEEE) is joined the Broadcasting System Research Group at the Electronics and Telecommunication Research Institute (ETRI) in 2002. He is responsible for terrestrial broadcasting standardization as well as HW/SW implementation and laboratory and field testing. He is a Principal Research Staff Member and currently leads multiple digital television (DTV)–related research projects. His research interests include error correction codes and digital communications, with a particular focus on signal processing technologies for digital television. He has authored and co-authored more than 350 peer-reviewed journal and conference papers. He has received numerous international and national honors, including the Richer Industry Leadership Medal from 2024, the two Prime Minister's Awards of Korea from 2019 to 2024, the two Scott Helt Memorial Awards from 2009 to 2019, more than ten BMSB Best Paper Awards, the KBS President's Award from 2022, and the two Best 100 National Research and Development Awards of Korea from 2019 to 2025. He currently serves as an Associate Editor of IEEE TRANSACTIONS ON BROADCASTING and *ETRI Journal*, and as a Distinguished Lecturer of the IEEE Broadcasting Technology Society. He is also the Chair of the IEEE BTS Daejeon Chapter and a member of the IEEE BMSB International Steering Committee.